Caloric Restriction and the TORC1-Sch9 Nutrient-Signaling Branch Link Chronological Aging to Cellular Quiescence in Yeast *Saccharomyces cerevisiae*

Tala Tafakori

A Thesis
in
The Department
of
Biology

Presented in Partial Fulfillment of the Requirements
for the Degree of Master of Science (Biology) at
Concordia University
Montreal, Quebec, Canada

August 2021

CONCORDIA UNIVERSITY

School of Graduate Studies

This is to certify that the Thesis prepared

By: Tala Tafakori

Entitled: Caloric Restriction and the TORC1-Sch9 Nutrient-Signaling Branch Link Chronological Aging to Cellular Quiescence in Yeast *Saccharomyces cerevisiae*

and submitted in partial fulfillment of the requirements for the degree of

Master of Sciences (Biology)

complies with the regulations of the University and meets the accepted standards with respect to originality and quality.

Signed by the final examining committee:

_____ Chair

Dr. Madoka Gray-Mitsumune

_____ External Examiner

Dr. Jin Suk Lee

_____ Examiner

Dr. Madoka Gray-Mitsumune

_____ Examiner

Dr. William Zerges

_____ Supervisor

Dr. Vladimir Titorenko

Approved by _____

Dr. Robert Weladji, Graduate Program director

_____

Dr. Pascal Sicotte, Dean of Faculty of Arts and Science

Date _____

ABSTRACT

Caloric Restriction and the TORC1-Sch9 Nutrient-Signaling Branch Link Chronological Aging to Cellular Quiescence in Yeast *Saccharomyces cerevisiae*

Tala Tafakori

Based on the recent findings of the Titorenko laboratory, I hypothesized that caloric restriction slows the chronological aging of budding yeast *Saccharomyces cerevisiae* because this geroprotective dietary intervention is integrated into the four processes of a cellular quiescence program. Limitation of calories prolongs yeast longevity by altering the properties of quiescent cells through an intricate network of nutrient-signaling pathways. In addition, I propose that genetic interventions inferring mutations in the Target of Rapamycin Complex 1 (TORC1)-Serine/threonine-protein kinase (Sch9) nutrient signaling branch (such as the *tor1Δ* and *sch9Δ* mutations) display longevity-extending phenotypes as a caloric restriction by targeting the processes of the quiescence program. In this study, caloric restriction and the mutant phenotypes of *sch9Δ* (in some cells) demonstrated a deceleration of yeast chronological aging by arresting the cell cycle in early G_1 and stimulating the development of high-density quiescent cells (process 1), whereas the phenotypes of the *tor1Δ* and the *sch9Δ* mutants (in some cells) displayed cell cycle arrest in late G_1, developing high-density quiescent cells. Caloric restriction promoted an aging-associated conversion of high-density quiescent cells into low-density quiescent cells (process 2), while the phenotypes of the *tor1Δ* and the *sch9Δ* mutants (in some cells) postponed the conversion of high-density quiescent cells into low-density quiescent cells. Therefore, yeast longevity can be extended by either promoting or decelerating process 2 of the quiescence program. The three interventions displayed a common effect in which they slowed down a fast aging-associated deterioration in clonogenicity of low-density quiescent cells (process 3) and postponed a slow aging-associated decline in clonogenicity of high-density quiescent cells (process 4).

Acknowledgments

I am deeply grateful to my supervisor Dr. Titorenko for his continuous guidance and support throughout my graduate studies in his laboratory. I would like to thank my committee members Dr. Madoka Gray-Mitsumune and Dr. William Zerges for their valuable suggestions that contributed to my research and learning experience, as well as current and past members of the Titorenko lab for their support. I would also like to thank Dr. Chris Law, from the Centre of Microscopy and Cellular Imaging, for his teachings and expertise, which greatly contributed to my research project.

Table of Contents

List of Figures

List of Abbreviations

Non-CR, non-caloric restriction; **CR**, caloric restriction; **Q**, quiescent; **NQ**, non-quiescent; **HD**, high density; **LD**, low density; **L**, logarithmic; **D**, diauxic; **PD**, post-diauxic; **ST**, stationary; **CFU**, colony forming units; **IPODs**, perivacuolar insoluble protein deposits; **PSGs**, proteasome storage granules; **RCD**, regulated cell death; **ROS**, reactive oxygen species; **TORC1**, target of rapamycin; **PKA**, protein kinase A; **Snf1**, sucrose non-fermenting complex 1; **Pho85**, phosphate metabolism protein 85; **Mpk1**, mitogen-activated protein kinase type 1; **Rim15**, regulator of IME2 protein 15; **Sch9**, *S. cerevisiae* homolog protein 9; **Yak1**, yet another kinase 1; **Mck1**, meiosis and centromere regulatory kinase 1; **Msn2/4**, multicopy suppressors 2 and 4 of SNF1 mutation; **Gis1**, Gig1-2 suppressor 1; **Hsf1**, heat shock transcription factor 1; **Gln3**, glutamine metabolism protein 3; **Gsy2**, glycogen synthase protein 2; **Atg1/13**, autophagy-related proteins 1 and 13; **Sfp1**, split-finger protein 1; **eIF2α**, translation initiation factor 2α; **Crz1**, calcineurin-responsive Zinc finger protein 1; **TAG**, neutral lipids triacylglycerols; **CL**, cardiolipin; **IMM**, inner mitochondrial membrane; $\Delta\Psi_m$, mitochondrial membrane potential; **mtDNA**, mitochondrial DNA; **PCD**, programmed cell death; **RCD**, regulated cell death; **YEPD**, 1% yeast extract + 2% peptone + 2% or 0.2% glucose.

Chapter 1: Introduction

1.1 Cellular metabolism and cell cycle regulation in *S. cerevisiae* not limited in the supply of calories.

When the budding yeast *Saccharomyces cerevisiae* is cultured in a nutrient-rich (complete) or synthetic (minimal) medium containing 2% glucose as the only carbon source at the beginning of culturing, the supply and intake of calories is sufficient to support growth, asymmetric division and survival of yeast cells for a certain period of time (Longo et al., 2012; Arlia-Ciommo et al., 2014). Therefore, these culturing conditions are referred to as non-caloric restriction (non-CR) (Goldberg et al., 2009; Arlia-Ciommo et al., 2014). By the end of the logarithmic growth phase under non-CR conditions, cultured *S. cerevisiae* consumes all exogenous glucose by fermentation (Goldberg et al., 2009; Fraenkel, 2011). At this time, the growth rate decreases, and cells enter a diauxic shift period (Goldberg et al., 2009; Fraenkel, 2011). The product of fermentation, ethanol, is then catabolized by aerobic respiration during the diauxic shift under non-CR conditions (Goldberg et al., 2009; Arlia-Ciommo et al., 2014). The growth rate is further decreased, and the culture enters a post-diauxic (PD) period, characterized by a high mitochondrial respiration rate (Goldberg et al., 2009; Arlia-Ciommo et al., 2014). Most of the cells within *S. cerevisiae* culture under non-CR arrest their cell cycle at the end of the PD period upon depletion of ethanol (Allen et al., 2006; Werner-Washburne et al., 2012). This cell cycle arrest happens at the nutrient-dependent checkpoint "START A" in the late G_1 phase (Allen et al., 2006; Werner-Washburne et al., 2012). Soon after the cell cycle arrest in the late G_1 phase, two cell populations become detectable in the non-CR culture. The names "quiescent (Q)" and "non-quiescent (NQ)" were coined to describe these cell populations (Allen et al., 2006; Werner-Washburne et al., 2012). The Q and NQ cell populations present in the non-CR cultures exhibit different physical, morphological, reproductive, biochemical and physiological properties (Allen et al., 2006; Werner-Washburne et al., 2012; Sagot et al., 2019; see below). The development and maintenance of these properties are governed by a complex nutrient-sensing signaling network that integrates various pathways and regulates many longevity-defining cellular processes (De Virgilio, 2012; Conrad et al., 2014).

1.2 Chronological aging of budding yeast cultured under non-CR conditions.

Many cells under non-CR whose cell cycle is arrested in the late G_1 phase at the end of the PD shift period enter a G_0 state of quiescence (Allen et al., 2006; Werner-Washburne et al., 2012; Leonov et al., 2017). Then, the entire non-CR culture reaches the stationary (ST) growth phase, and the process of chronological aging begins (Fraenkel, 2011; Longo et al., 2012; Arlia-Ciommo et al., 2014). The rate of chronological aging in budding yeast is assessed by the length of time during which a yeast cell preserves a G_0 state of quiescence (Figure 1.1) (Longo et al., 2012; Arlia-Ciommo et al., 2014). A clonogenic plating assay is commonly used to evaluate a chronological aging-associated loss of the G_0 state of quiescence (Longo et al., 2012; Arlia-Ciommo et al., 2014). In the clonogenic plating assay, aliquots of a non-CR yeast culture are recovered on different days after the culture enters the ST phase and are plated on the surface of Petri dishes with a solid nutrient-rich medium (Longo et al., 2012; Arlia-Ciommo et al., 2014). A cell in the culture that retains high viability is a Q cell in the G_0 state (Figure 1.1) (Longo et al., 2012; Arlia-Ciommo et al., 2014). Notably, it is a common belief that the same general principles underlying the chronological aging in budding yeast also mimic the aging of post-mitotic Q cells (such as neurons or myocytes) in multicellular eukaryotes (Longo et al., 2012; Arlia-Ciommo et al., 2014).

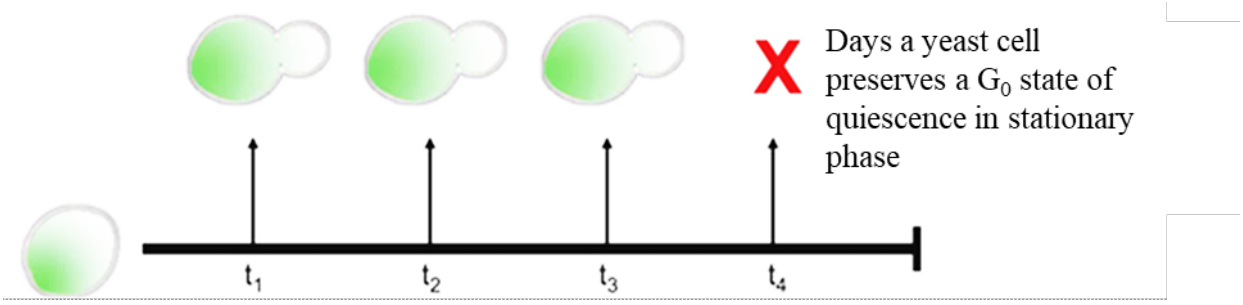

Figure 1.1: Measuring the rate of chronological aging in *S. cerevisiae*. A clonogenic plating assay examines how long cells within the stationary-phase culture maintain the G0 state of quiescence during chronological aging. From Kaeberlein et al., Recent Developments in Yeast Aging, 2007.

1.3 An outline of the cellular quiescence program that operates in *S. cerevisiae* cultured under non-CR conditions.

The physical, morphological, reproductive, biochemical and physiological properties characteristic of the Q and NQ yeast cells under non-CR is developed and maintained by a cellular quiescence program (Aragon et al., 2008; Davidson et al., 2011; Werner-Washburne et al., 2012; Miles et al., 2013; Sagot et al., 2019). Budding yeast under non-CR starts entering the cellular quiescence program during the diauxic period of growth in response to nutrient deprivation (Aragon et al., 2008; Davidson et al., 2011; Werner-Washburne et al., 2012; Miles et al., 2013). The program continues during the subsequent stationary (ST) phase of culturing when the process of chronological aging begins (Aragon et al., 2008; Davidson et al., 2011; Werner-Washburne et al., 2012; Miles et al., 2013). A body of evidence indicates that the development of the cellular quiescence program during the ST phase defines the pace of chronological aging in *S. cerevisiae* under non-CR by orchestrating specific longevity-defining cellular processes (Aragon et al., 2008; Davidson et al., 2011; Werner-Washburne et al., 2012; Miles et al., 2013; Leonov et al., 2017). A signaling network of yeast quiescence defines an age-related spatiotemporal organization of these cellular processes (Smets et al., 2010; De Virgilio, 2012; Conrad et al., 2014). As any other multi-step biological program, this program provides specific benefits to the environmental adaptation, stress resistance development and long-term survival of yeast inhabited in a particular ecosystem (Smets et al., 2010; De Virgilio, 2012; Werner-Washburne et al., 2012; Palková et al., 2014; Gulli et al., 2019; Sagot et al., 2019).

1.4 The Q and NQ cells present within yeast cultures under non-CR conditions differ in their properties.

Glucose depletion triggers a cascade of signaling events leading to the formation of Q and NQ cell populations within a non-CR culture. The Q cells arise from the cells whose cell cycle is arrested in the late G_1 phase at the end of the PD shift, while the cells whose cell cycle is not arrested create the NQ 1 cell population. The NQ 1 cells are converted into the NQ 2 and NQ 3 cells in two consecutive steps (Figure 1.2). Also, as the Q cells chronologically age, they progressively convert into NQ 1 cells, thereby contributing to the replenishment of the NQ 2 and NQ 3 cell pools (red arrow in figure 1.2) (Werner-Washburne et al., 2012). Because the Q and NQ cells exhibit different properties such as density, they can be purified using Percoll density gradient centrifugation (Figure 1.2) (Allen et al., 2006; Aragon et al., 2008; Davidson et al., 2011; Werner-

Washburne et al., 2012; Miles et al., 2013; Leonov et al., 2017; Sagot et al., 2019). In sum, glucose depletion causes the formation of two cell populations, namely Q and NQ 1, leading to the stepwise formation of NQ 2 and NQ 3 cells in an age-dependent manner.

The Q cells recovered from the non-CR culture have distinct properties that distinguish them from NQ cells. At least some or all of the Q cell properties outlined in Figure 1.2 allow them to retain viability for a longer time during the chronological lifespan (CLS). Q cells are unbudded daughter cells of high buoyant density, uniformly sized, surrounded by a thick cell wall, and refract light when viewed by phase-contrast microscopy. They exhibit a high rate of metabolism, elevated mitochondrial respiration, increased electrochemical potential across the inner mitochondrial membrane, have a low concentration of mitochondrially produced reactive oxygen species (ROS), contain low extend of ROS-induced macromolecular damage, and maintain a low mutation rate. Another characteristic of quiescence is the high concentration of glycogen and trehalose, the two glucose stores of yeast cells whose intracellular concentrations rise when nutrient supplies decline. Moreover, the clonogenic plating assay and the synchronous division assay distinguish the presence of Q cells from NQ cells by assessing their high viability capacities and their ability to synchronously re-enter the mitotic cycle, respectively. Q cells are highly resistant to chronic thermal and oxidative stresses applied exogenously. These cells exhibit postponed onsets of the age-related forms of regulated apoptotic and necrotic cell death (Allen et al., 2006; Aragon et al., 2008; Davidson et al., 2011; Werner-Washburne et al., 2012; Miles et al., 2013; Leonov et al., 2017; Sagot et al., 2019). Additionally, the subcellular distribution and water-solubility state of heat-shock proteins in the Q cells are dynamically unstable, where some heat-shock proteins are confined to multiple water-insoluble foci and filaments in the cytosol, and others relocate from the cytosol to the nucleus. Cells in the Q state exhibit altered nuclear morphology; the chromosomes in the nucleus of these cells and transcriptional profiles of their nuclear genes undergo characteristic changes. Q cells maintain a high proteostasis capacity which includes the build-up of the cytosolic P-bodies and stress granules, relocation of dysfunctional proteasome subunits from the nucleus to the perivacuolar insoluble protein deposits (IPODs), and the movement of functional proteasome subunits from the nucleus to the proteasome storage granules (PSGs) in the cytosol. A substantial reorganization of the actin- and microtubule-based cytoskeleton structures is yet another characteristic property of the Q cells. The dynamic mitochondrial network in these cells is fragmented, and many small globular mitochondrial structures amass at the cell periphery (Sagot et al., 2019). Although the mechanisms by which the development and maintenance of these

properties are largely unknown, at least some of the above characteristics of Q cells contribute to their known abilities to exit a G_0 state of quiescence, re-enter the mitotic cell cycle and proliferate. As such, these properties define the pace of chronological aging in budding yeast.

The three NQ cell populations exhibit a distinct array of properties, differentiating them from the Q cells present in the same culture under non-CR. The NQ 1 cells are mainly first- and higher generation mother cells of low buoyant density, most of these cells are budded and are replicatively old as their surface shows one or more bud scars. Akin to the Q cells, the NQ 1 cells are metabolically active, clonogenic and can synchronously re-enter mitosis if nutrients are re-supplied. Unlike the Q cells, the NQ 1 cells exhibit a low rate of mitochondrial respiration, amass bulk quantities of ROS, and display high mutation rates in both nuclear and mitochondrial DNA (Allen et al., 2006; Aragon et al., 2008; Davidson et al., 2011; Werner-Washburne et al., 2012; Miles et al., 2013; Leonov et al., 2017; Sagot et al., 2019). These properties of the NQ 1 cells support the notion that most of them are direct descendants of the Q cells becoming chronologically older (Washburne et al., 2012). The NQ 2 cells are budded mother cells of low buoyant density, covered with bud scars. These cells are direct descendants of the NQ 1 cells that get chronologically older by losing their clonogenicity and becoming incapable of re-entering mitosis synchronously if nutrients are re-supplied. Reminiscent of the NQ 1 cells, the NQ 2 cells exhibit a high rate of cellular metabolism and impaired mitochondrial respiration (Allen et al., 2006; Aragon et al., 2008; Davidson et al., 2011; Werner-Washburne et al., 2012; Miles et al., 2013). The chronological aging of the NQ 2 cells yields the NQ 3 cells. Like their direct ancestors, the NQ 3 cells are non-clonogenic and incapable of re-entering mitosis synchronously if nutrients are re-supplied. Unlike their direct ancestors, the NQ 3 cells display major hallmarks of the apoptotic and necrotic forms of regulated cell death (RCD) (Allen et al., 2006; Aragon et al., 2008; Davidson et al., 2011; Werner-Washburne et al., 2012; Miles et al., 2013). The comparative analysis of the Q and NQ cell characteristics suggests that the loss of some or all of the Q properties in a stepwise age-dependent manner results in the loss of viability of these cells, thus diminishing the chronological lifespan.

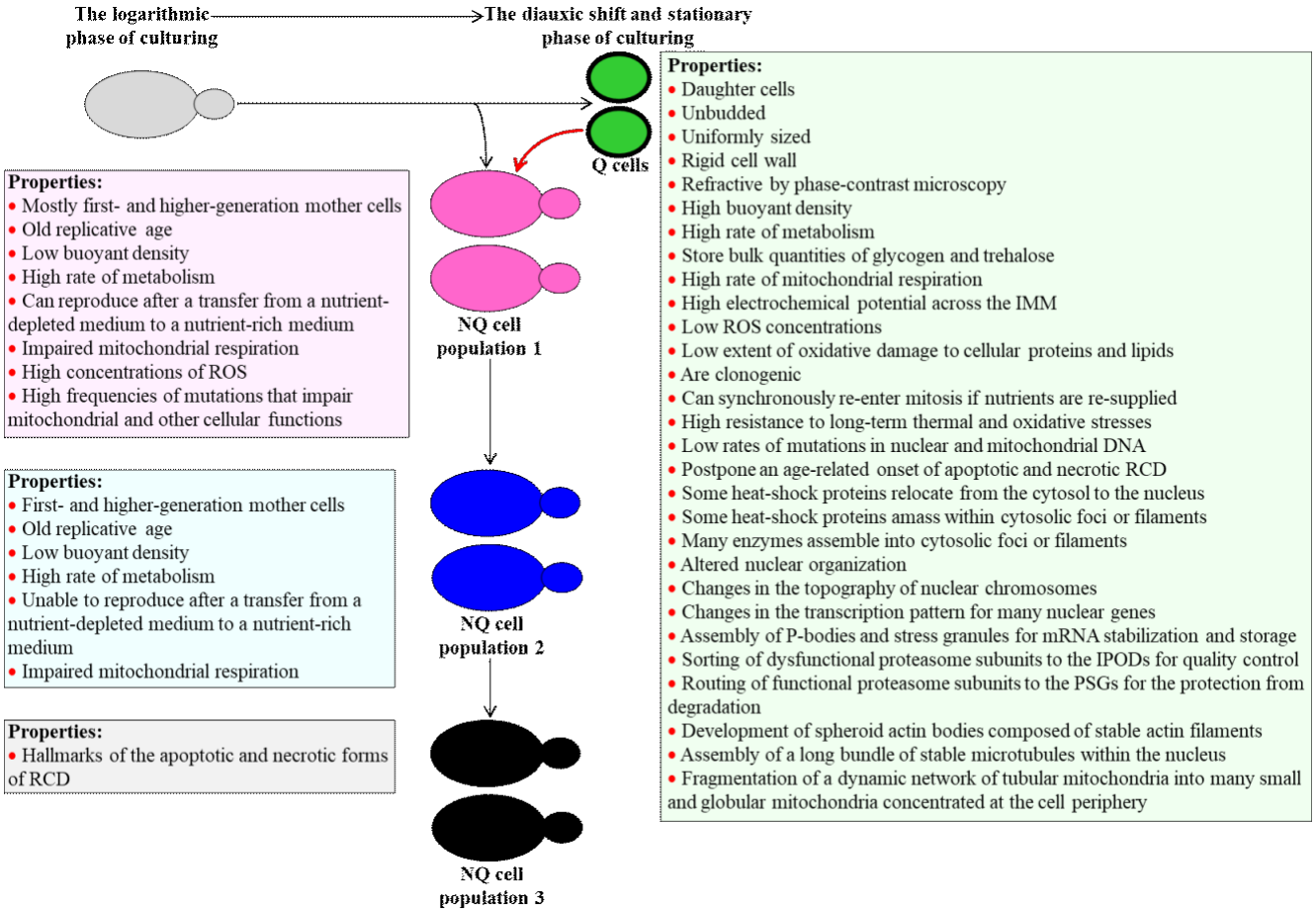

Figure 1.2: During a PD shift period, the non-CR culture of *S. cerevisiae* yeast begins to accumulate the populations of Q and NQ cells. The Q cells originate from those daughter cells in the culture whose cell cycle is arrested in the late G_1 phase; after cell cycle arrest, these cells enter a G_0 state of quiescence. These Q cells develop and maintain a distinct set of properties named in the figure. The NQ cells originate from those mother cells in the culture whose cell cycle is not arrested in the late G_1 phase; a pool of the NQ cells also consists of chronologically old descendants (a red arrow) of the Q cells. The NQ cell populations 2 and 3 are direct (the NQ 2 cells) or indirect (the NQ 3 cells) descendants of the NQ 1 cell population. The physical, morphological, reproductive, biochemical and physiological properties of the Q and NQ cells are different. See the text for more details. From Mohammad, K. et al., 2020, Mechanisms that Link Chronological Aging to Cellular Quiescence in Budding Yeast, 2020.

1.5 Nutrient-sensing signaling networks control the cellular quiescence program by regulating longevity-defining processes in the Q and NQ cells under non-CR conditions.

A complex nutrient-sensing signaling network directs the formation and conversion of the Q, NQ 1, NQ 2 and NQ 3 cell populations in *S. cerevisiae* under non-CR (Figure 1.3). This signaling network contributes to the establishment, maintenance and evolution of the cellular quiescence program. Four protein complexes operate as the core hubs of the network. These nutrient-sensing protein complexes include a target of rapamycin complex 1 (TORC1), protein kinase A (PKA), sucrose non-fermenting complex 1 (Snf1) and phosphate metabolism protein 85 (Pho85) (Smets et al., 2010; De Virgilio, 2012; Conrad et al., 2014; Swinnen et al., 2014; Deprez et al., 2018; Miles et al., 2019; Zhang et al., 2019). TORC1, PKA, Snf1 and Pho85 perform a phosphorylative activation or inactivation of a subset of proteins that act as the key nodes of the network. A distinct family of protein kinases, transcription activators, translation initiation factors and metabolic enzymes are among the network's key nodes. These key nodes include a mitogen-activated protein kinase type 1 (Mpk1), a regulator of IME2 protein 15 (Rim15), an *S. cerevisiae* homolog protein 9 (Sch9), a yet another kinase 1 (Yak1), a meiosis and centromere regulatory kinase 1 (Mck1), the multicopy suppressors 2 and 4 of SNF1 mutation (Msn2/4), a Gig1-2 suppressor 1 (Gis1), a heat shock transcription factor 1 (Hsf1), a glutamine metabolism protein 3 (Gln3), a glycogen synthase protein 2 (Gsy2), the autophagy-related proteins 1 and 13 (Atg1/13), a split-finger protein 1 (Sfp1), a translation initiation factor 2α (eIF2α) and a calcineurin-responsive Zinc finger protein 1 (Crz1) (Smets et al., 2010; De Virgilio, 2012; Conrad et al., 2014; Swinnen et al., 2014; Deprez et al., 2018; Miles et al., 2019; Zhang et al., 2019). Each of the network's key nodes is linked to downstream nodes of the signaling network contributing to the establishment, maintenance and evolution of the cellular quiescence program, where they play essential roles in defining the pace of chronological aging in *S. cerevisiae.*

An increase in nitrogen or carbon source availability activates the protein kinase activity of TORC1 (Figure 1.3). The TORC1-dependent phosphorylation stimulates or inhibits the network's key nodes Mpk1, Rim15, Sch9, Mck1, Msn2/4, Gln3, Gsy2, Atg1/13, Sfp1 and eIF2α9. After being stimulated or inhibited by TORC1, these key nodes of the network cause a global reorganization of many downstream nodes. These downstream nodes have been implicated in cell growth, mitotic division, cell wall maintenance, stress resistance, trehalose and glycogen metabolism, metabolism and transport of alternative nitrogen sources, proteostatic quality control, various forms of selective and non-selective autophagy, ROS homeostasis, ribosome biogenesis

and translational initiation (Smets et al., 2010; De Virgilio, 2012; Conrad et al., 2014; Swinnen et al., 2014). One of the network's key nodes phosphorylated and stimulated by TORC1 is the serine-threonine protein kinase Sch9 (Swinnen et al., 2014; Deprez et al., 2018). At the beginning of cell culturing under non-CR, the TORC1-dependent stimulation of Sch9 enhances transcription of genes involved in ribosome biogenesis, advances the initiation of protein synthesis and suppresses transcription of stress response genes; this slows cell entry into quiescence, suppresses quiescence maintenance and shortens the CLS. At the diauxic shift period, glucose depletion inhibits TORC1 and Sch9 to promote quiescence and extend CLS. Therefore, nutrient availability stimulates the TORC1 pathway, which signals downstream nodes, regulating some longevity-defining properties (Smets et al., 2010; De Virgilio, 2012; Conrad et al., 2014; Swinnen et al., 2014).

A rise in the carbon, nitrogen or phosphate source availability activates the PKA core hub of the nutrient signaling network (Figure 1.3). The PKA-dependent phosphorylation stimulates or inhibits the network's key nodes Rim15, Yak1, Mck1, Msn2/4, Gsy2, Atg1/13, Sfp1 and Crz1. These key nodes regulate the network's downstream nodes involved in cell survival, mitotic division, transcription of stress response genes, trehalose and glycogen metabolism, autophagy, protection of specific mRNAs, ribosome biogenesis, ROS homeostasis and Ca^{2+} homeostasis maintenance. Many of these cellular processes are essential contributors to quiescence and longevity assurance regulated by PKA in response to nutrient availability (Smets et al., 2010; De Virgilio, 2012; Conrad et al., 2014).

The Snf1 heterotrimeric protein complex phosphorylates, activates, or inactivates the network's key nodes Msn2/4, Hsf1, Gln3, Gsy2, Atg1/13 and eIF2α in response to glucose depletion (Figure 1.3). The network's downstream processes include transcription of stress response genes, ROS homeostasis maintenance, vesicular protein trafficking, cell wall maintenance, metabolism and transport of alternative nitrogen sources, glycogen metabolism, autophagy, and protein synthesis initiation. Thus, several processes implicated in both quiescence and longevity regulation of CLS are governed by the Snf1 pathway in response to glucose levels (De Virgilio, 2012; Conrad et al., 2014; Shashkova et al., 2015).

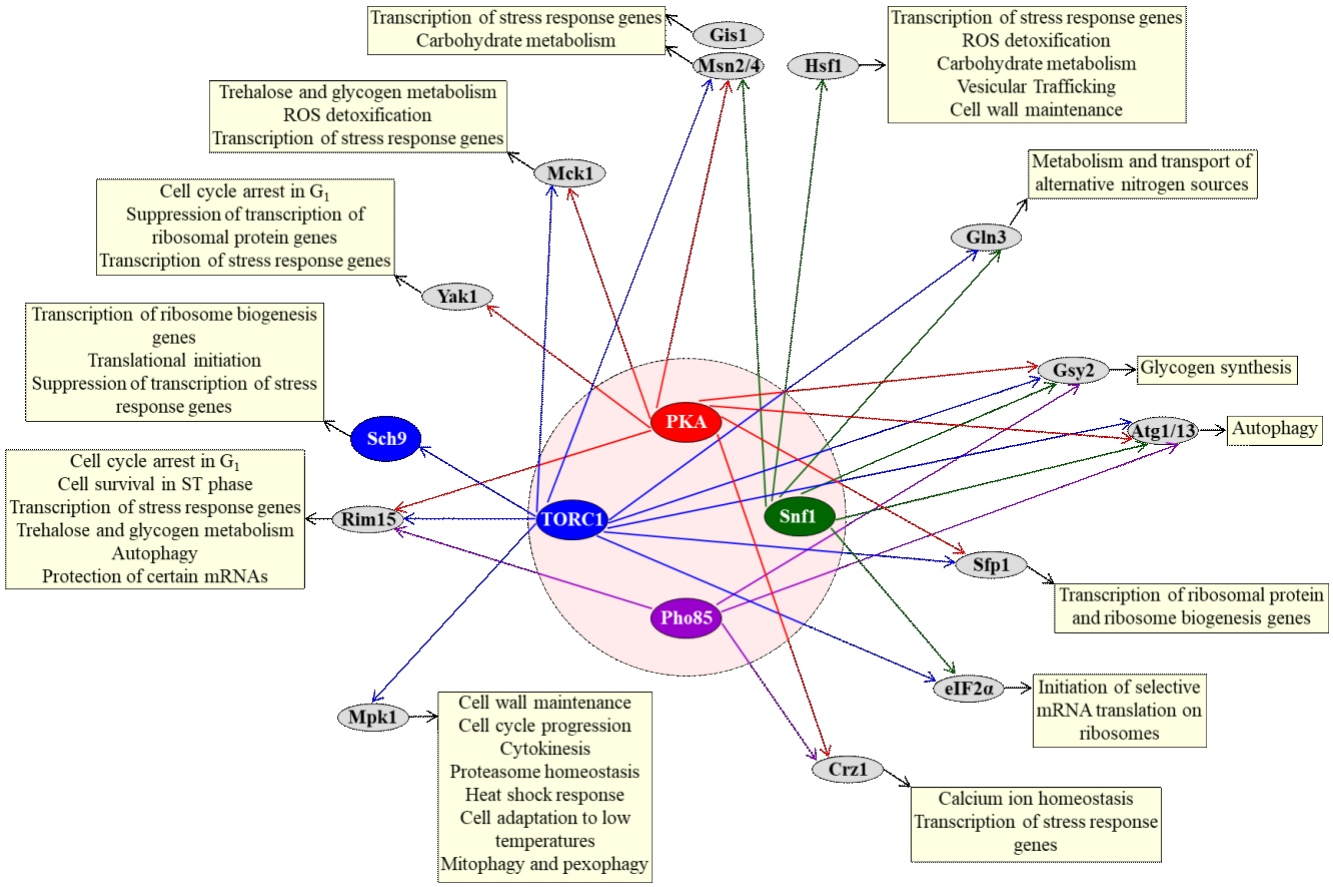

Figure 1.3: A nutrient-sensing signaling network controls the processes implicated in both cellular quiescence and longevity assurance of chronologically aging *S. cerevisiae* under non-CR. The protein complexes target of rapamycin complex 1 (TORC1), protein kinase A (PKA), sucrose non-fermenting complex 1 (Snf1) and phosphate metabolism protein 85 (Pho85) are the core hubs of the network. TORC1, PKA, Snf1 and Pho85 perform a phosphorylative activation or inactivation of a subset of proteins that act as the key nodes of the network. These key nodes include a mitogen-activated protein kinase type 1 (Mpk1), a regulator of IME2 protein 15 (Rim15), an *S. cerevisiae* homolog protein 9 (Sch9), a yet another kinase 1 (Yak1), a meiosis and centromere regulatory kinase 1 (Mck1), the multicopy suppressors 2 and 4 of SNF1 mutation (Msn2/4), a Gig1-2 suppressor 1 (Gis1), a heat shock transcription factor 1 (Hsf1), a glutamine metabolism protein 3 (Gln3), a glycogen synthase protein 2 (Gsy2), the autophagy-related proteins 1 and 13 (Atg1/13), a split-finger protein 1 (Sfp1), a translation initiation factor 2α (eIF2α) and a calcineurin-responsive Zinc finger protein 1 (Crz1). Each of the network's key nodes is linked to the downstream nodes (cellular processes) that contribute to establishing, maintaining, and evolving the cellular quiescence program and longevity assurance under non-CR conditions. See the text for more details. From Mohammad, K. et al., 2020, Mechanisms that Link Chronological Aging to Cellular Quiescence in Budding Yeast, 2020.

The Pho85 core hub protein of the cellular signaling network is a cyclin-dependent protein kinase bound to several Pho80 cyclin family members (Figure 1.3). The Pho80 cyclin-bound form of Pho85 phosphorylates and inactivates specific protein targets known as the network's key nodes Rim15, Gsy2, Atg1/13 and Crz1. When carbon and phosphate sources become limited, the Pho85-dependent phosphorylative inactivation of Rim15, Gsy2, Atg1/13 and Crz1 is suppressed, and these key nodes of the cellular quiescence signaling network become capable of regulating the network's downstream processes involved in the mitotic cell cycle regulation, bud site selection in G_1 phase, transcription of stress response genes, trehalose and glycogen metabolism, autophagy, sphingolipid formation, phosphate metabolism, cellular proteostasis, Ca^{2+} homeostasis maintenance, and actin cytoskeleton function. Many of these cellular processes regulated by Pho85 are known for their essential roles in quiescence maintenance and longevity assurance of chronologically aging in *S. cerevisiae* (Smets et al., 2010; De Virgilio, 2012; Conrad et al., 2014).

1.6 CR alters many properties of the Q and NQ cells and affects the age-related dynamics of their development during the chronological aging of *S. cerevisiae.*

CR is a robust and evolutionarily conserved aging-delaying (geroprotective) dietary intervention that prolongs longevity in budding yeast and other eukaryotes (Sinclair, 2005; Madeo et al., 2019). The effect of CR on chronological aging is usually investigated in *S. cerevisiae* cultured in a nutrient-rich complete or nutrient-limited synthetic minimal medium initially containing 0.2% or 0.5% glucose as the only carbon source (Longo et al., 2012; Arlia-Ciommo et al., 2014). When cultured in a nutrient-rich complete medium (YEPD) initially containing 0.2% or 0.5% glucose as the sole carbon source, cells are known to receive all nutrients needed to support growth and survival (Fraenkel, 2011). In addition, a body of evidence supports the notion that the use of this medium for culturing budding yeast provides several important advantages for understanding mechanisms through which CR slows the chronological aging of this eukaryote (Goldberg et al., 2009).

The Titorenko laboratory used Percoll density gradient centrifugation to purify the Q and NQ cells from budding yeast cultured in the YEPD medium initially containing 0.2% glucose (CR) or 2.0% glucose (non-CR) as the only carbon source (Leonov et al., 2017). The Q and NQ cells were purified from budding yeast taken on different days of culturing in these media to assess the chronological aging-associated dynamics of changes in cell properties (Leonov et al., 2017).

CR dynamically alters the properties of Q and NQ, where some or all of these changes may enhance longevity, which ultimately increases their CLS. *S. cerevisiae* cultured under non-CR that enter the G_0 state of quiescence arrest their cell cycle in late G_1, resulting in relatively large Q^{HD} cells (Figure 1.4A, right panel). When cultured under CR, formation of the Q^{HD} cells occur in an early G_1 cell cycle arrest, resulting in relatively smaller cells (Figure 1.4A, left panel) (Allen et al., 2006; Aragon et al., 2008; Davidson et al., 2011; Werner-Washburne et al., 2012; Miles et al., 2013; Leonov et al., 2017). CR also alters the timing of the Q^{HD}-to-Q^{LD} cell conversion in the culture of chronologically aging yeast, where the maximal percentage of Q^{LD} cells under non-CR is observed at the ST growth phase (Figure 1.4B, right panel). Yet, under CR, the percentage of Q^{LD} cells reaches a maximum in the PD growth phase (Figure 1.4B, right panel). CR Q and NQ cells sustain viability and their ability to re-enter the mitotic cell cycle for a more extended time as opposed to non-CR cells (Figure 1.4C and 1.4D) (Leonov et al., 2017).

The intracellular concentrations of several metabolites, which play essential roles in chronological aging, have been shown to change in response to CR. A rise of intracellular glycogen concentration in the Q and NQ cells occurs when cells are limited in calories (Figure 1.4E); This high-molecular-mass multibranched polysaccharide of glucose serves as a form of energy storage in budding yeast cells (François and Parrou, 2001). CR also elevates the intracellular concentration of trehalose in the Q and NQ cells (Figure 1.4E) (Leonov et al., 2017); This nonreducing disaccharide consists of two molecules of glucose and is used for preserving energy (François and Parrou, 2001), maintaining cellular proteostasis (Kyryakov et al., 2012) and protecting budding yeast from death inflicted by exposure to various environmental chronic stresses (Kyryakov et al., 2012). CR lowers the intracellular concentrations of the neutral lipids triacylglycerols (TAG) in Q and NQ cells (Figure 1.4F); TAG is initially formed in the endoplasmic reticulum (ER) and then accumulated in lipid droplets (LD) as the fatty acid reserves for energy production and phospholipid synthesis (Leonov et al., 2017; Mitrofanova et al., 2018). CR induces a substantial rise in the intracellular concentrations of the signature mitochondrial membrane, diphosphatidylglycerol lipids cardiolipins (CL), in the inner mitochondrial membrane (IMM) of Q and NQ cells (Figure 1.4G); CL perform the essential pro-longevity roles in chronologically aging budding yeast because these lipids protect mitochondria from the age-related morphological changes and functionality decline (Leonov et al., 2017; Mitrofanova et al., 2018).

Under CR, Q and NQ cells exhibit a considerable increase in mitochondrial respiration and the electrochemical potential across the IMM ($\Delta\Psi_m$) (Figure 1.4H) (Leonov et al., 2017). These

CR effects on mitochondrial functionality are essential contributors to the CR-dependent deceleration of the chronological aging in budding yeast (Leonov and Titorenko., 2013; Beach et al., 2015). In the chronologically "young" Q and NQ cells that did not enter the ST growth phase, CR lowers the intracellular ROS (Figure 1.4I) (Leonov et al., 2017). However, after the Q and NQ cells enter the ST growth phase and become chronologically "old," CR raises the intracellular ROS (Figure 1.4I) (Leonov et al., 2017). ROS are the by-products of mitochondrial respiration that regulate the longevity of yeast in a concentration-dependent, hormetic manner (Giorgio et al., 2007; Goldberg et al., 2009; Leonov and Titorenko., 2013; Arlia-Ciommo et al., 2014; Beach et al., 2015; Dakik et al., 2019). The extent of oxidative damage to cellular proteins, lipids, and DNA in the nucleus and mitochondria is decreased during chronological aging of Q and NQ cells under CR (Figure 1.4J) (Leonov et al., 2017). The essential role of oxidative macromolecular damage as a chronological aging-accelerating factor in budding yeast is well known (Gladyshev et al., 2013; Leonov and Titorenko., 2013; Beach et al., 2015; Dakik et al., 2019; Ogrodnik et al., 2019).

The resistance of the Q and NQ cells to chronic (long-term) thermal and oxidative stresses is increased during the chronological aging of budding yeast under CR (Figure 1.4K). Increased resistance to these chronic stresses is an essential pro-longevity factor in chronological aging (Goldberg et al., 2009; Arlia-Ciommo et al., 2014; Leonov and Titorenko., 2013; Beach et al., 2015; Dakik et al., 2019). Furthermore, an age-related onset of the apoptotic and necrotic forms of regulated cell death (RCD) is postponed by CR (Figure 1.4L). Q and NQ cells cultured under CR become more resistant to these forms of RCD induced in response to exogenous pro-death chemical interventions (Figure 1.4M) (Leonov et al., 2017; Herker et al., 2004; Arlia-Ciommo et al., 2014; Richard et al., 2014; Sheibani et al., 2014).

In sum, CR-mediated changes in yeast appear to prolong viability during the CLS. At least some or all of these changes in the properties of Q and NQ induced by CR enhance their viability for a more extended time.

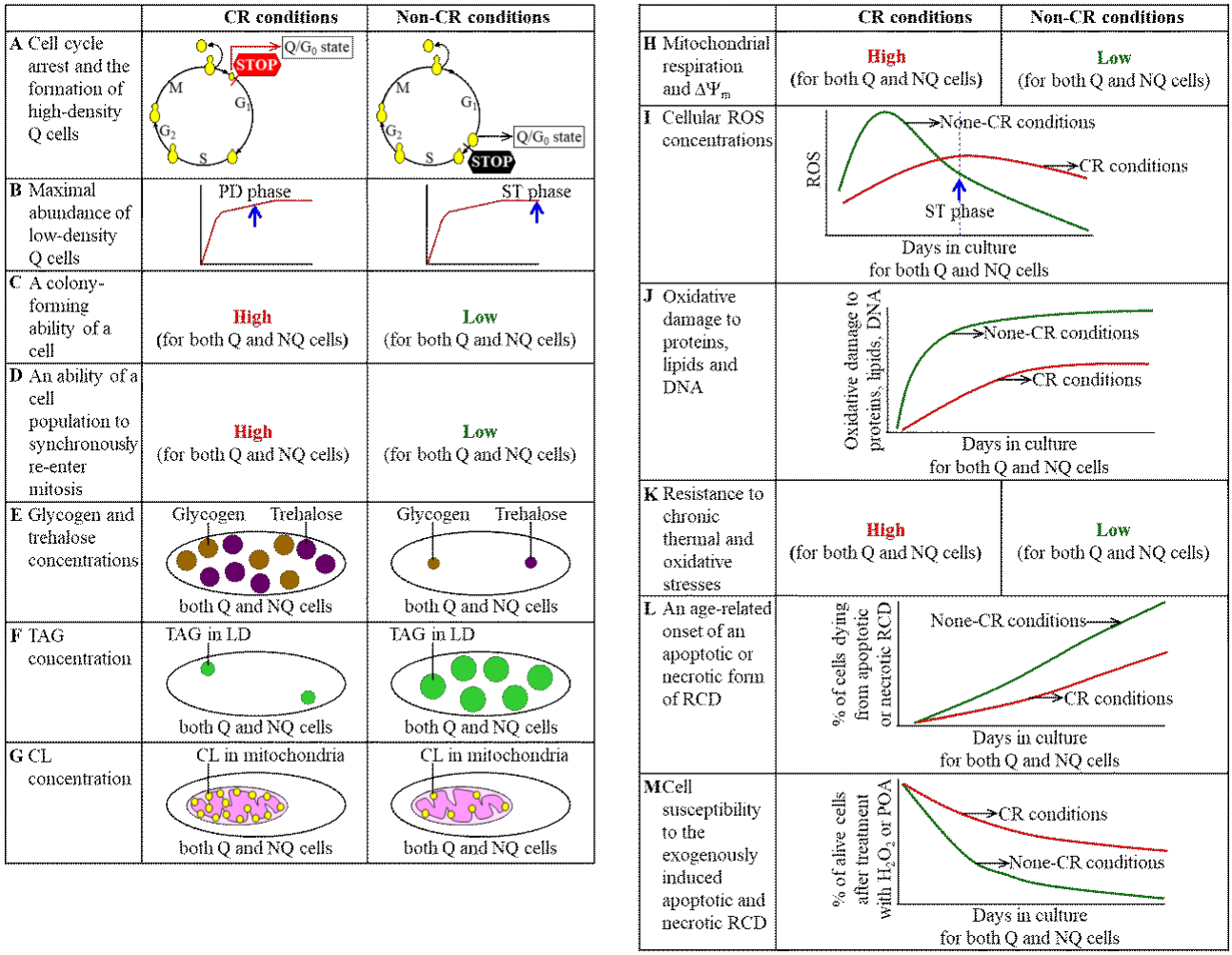

Figure 1.4: CR alters many properties of the Q and NQ cells and affects the cell cycle- or age-related dynamics of their development during the chronological aging of *S. cerevisiae*.

The properties of the Q and NQ cells or the cell cycle- or age-related development dynamics are named in panels **A-M**. Please see the text for more details. Abbreviations: CL, cardiolipins; LD, lipid droplets; POA, palmitoleic acid; RCD, regulated cell death; ROS, reactive oxygen species; TAG, triacylglycerols; $\Delta\Psi_m$, the electrochemical potential across the inner mitochondrial membrane. From Mohammad, K. et al., 2020, Mechanisms that Link Chronological Aging to Cellular Quiescence in Budding Yeast, 2020.

1.7 Hypothesis: Dietary intervention CR and genetic interventions *tor1Δ* and *sch9Δ* slow the chronological aging of *S. cerevisiae* because they target some or all four processes integrated into the cellular quiescence program.

Based on the above findings, I hypothesized that CR might decelerate the chronological aging of *S. cerevisiae* because this dietary intervention activates or inhibits specific nutrient signaling pathways whose downstream processes are integrated into the cellular quiescence program.

First, the hypothesis posits that during process 1 of the cellular quiescence program, CR slows the CLS because it arrests the cell cycle in early G_1 and creates small Q^{HD} cells instead of larger Q^{HD} cells under non-CR (Figure 1.5). Second, during process 2 of the quiescence program, CR delays aging because it promotes an accumulation of Q^{LD} cells as early as the PD phase instead of the ST phase of non-CR cells (Figure 1.5). Third, CR slows a transformation of long-lived Q^{LD} cells into short-lived NQ^{LD} cells during process 3 of the quiescence program (Figure 1.5). Fourth, CR decelerates a conversion of long-lived Q^{HD} cells into short-lived NQ^{HD} cells during process 4 of the quiescence program (Figure 1.5). It is feasible that these changes are essential contributors to the acquirement of some or all pro-longevity properties mentioned in Figure 1.5.

Genetic interventions, including mutations in the pro-longevity nutrient-sensing TORC1-Sch9 signaling branch (such as *tor1Δ* and *sch9Δ)*, exhibit phenotypes that slow the chronological clock (Figure 1.6). Therefore, I further extend my hypothesis by proposing that *tor1Δ* and *sch9Δ* mutations affect some or all of the four processes of the cellular quiescence program, similarly to CR (Figure 1.5 and the Results section). Choosing these mutants and assessing their phenotypes regarding the quiescence program may shed like onto the wild-type functions of these proteins on quiescence and longevity extension of the CLS in *S. cerevisiae.*

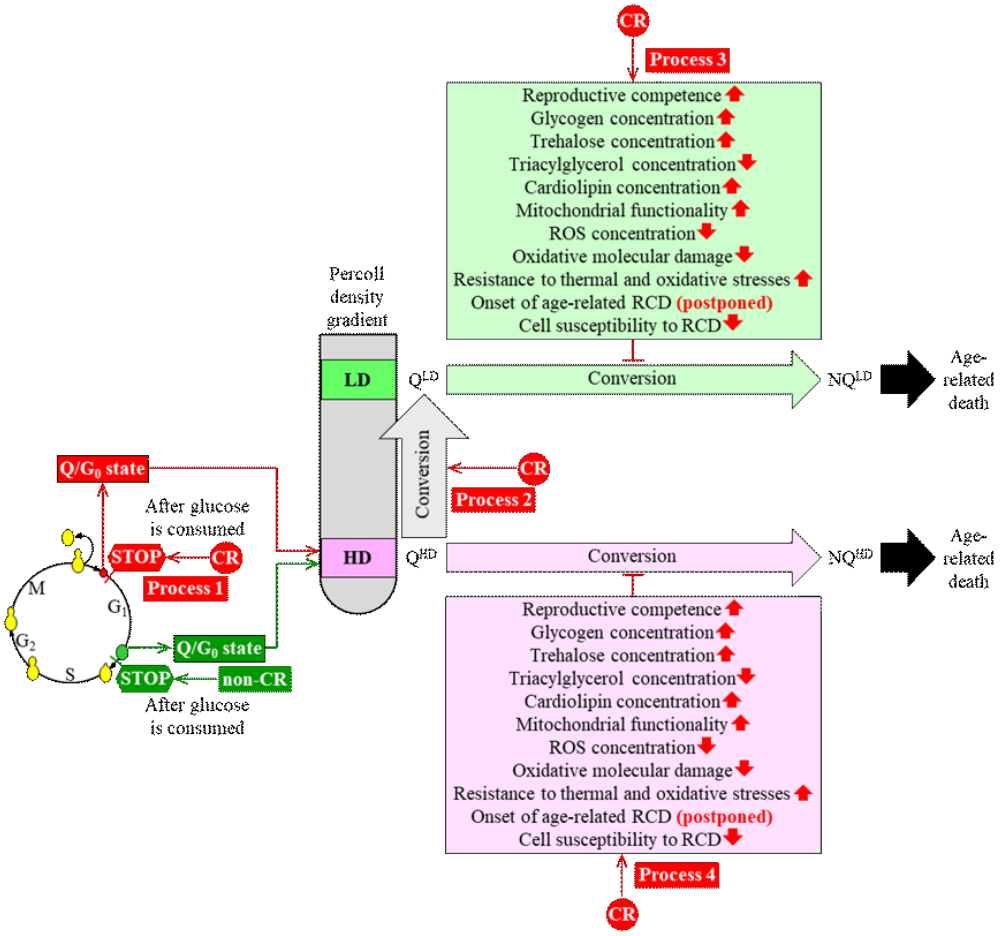

Figure 1.5: A hypothesis on how CR, *tor1Δ* and *sch9Δ* might slow the chronological lifespan of *S. cerevisiae* because these interventions target processes 1, 2, 3 and/or 4 integrated into the cellular quiescence program. See the text for more details. Abbreviations: HD, high-density cells; LD, low-density cells; Q^{HD}, quiescent cell of high density; Q^{LD}, quiescent cell of low density; NQ^{HD}, non-quiescent cell of high density; NQ^{LD}, non-quiescent cell of low density; RCD, regulated cell death; ROS, reactive oxygen species. ↑ Increased by CR; ↓ Decreased by CR; ⊣ Slows the conversion of Q^{LD} cells into NQ^{LD} cells or the Q^{HD}-to-NQ^{HD} cell transformation. From Mohammad, K. et al., 2020, Mechanisms that Link Chronological Aging to Cellular Quiescence in Budding Yeast, 2020.

1.8 The objectives of studies described in this thesis.

The objective of the studies was to test the hypothesis that dietary intervention, CR, and the genetic interventions, *tor1Δ* and *sch9Δ,* slow chronological aging by targeting the four processes integrated into the cellular quiescence program. To attain this objective, I compared the effects of CR, *tor1Δ* and *sch9Δ* by measuring the cell diameters of high density (HD) and low density (LD) cells to determine early or late cell cycle arrest in G1 (process 1), measuring the percentage of HD cells to assess the extent of LD cell accumulation (process 2), and determining the viability of HD and LD cells by evaluating their colony-forming capability (process 3 and 4, respectively).

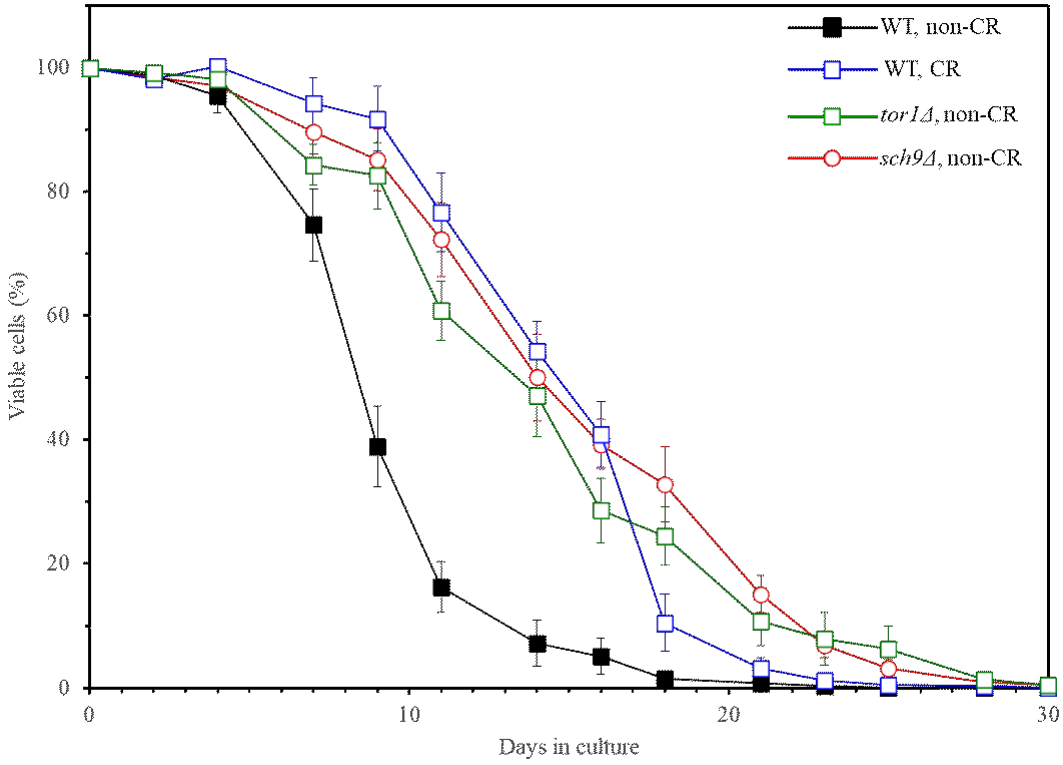

Figure 1.6. Survival curves of the wild-type (WT) and mutant strains *tor1Δ* and *sch9Δ* (in the WT genetic background) of *S. cerevisiae* cultured in the nutrient-rich YPD medium initially containing 0.2% glucose (CR) or 2% glucose (non-CR). The ability of a cell to form a colony on the surface of the nutrient-rich solid YPD medium with 2% glucose was used as a criterium of cell viability (See "Materials and Methods" section). Data are presented as means ± SEM (n = 3).

Chapter 2: Materials and Methods

2.1 Yeast strains, growth media and cell culture conditions.

The wild-type (WT) strain *Saccharomyces cerevisiae* BY4742 (*MATα his3Δ1 leu2Δ0 lys2Δ0 ura3Δ0*; "Thermo Scientific/Open Biosystems") was cultured in the liquid nutrient-rich YP medium. This medium contained 1% (w/v) yeast extract and 2% (w/v) peptone (both from "Fisher Scientific"). It was supplemented with 2% (w/v) glucose ("Fisher Scientific") or 0.2% (w/v) glucose as the only carbon source. The *tor1Δ* single-gene-deletion mutant strain or *sch9Δ* single-gene-deletion mutant strain (both in the BY4742 genetic background; "Thermo Scientific/Open Biosystems") was cultured in the liquid nutrient-rich YP medium supplemented with 2% (w/v) glucose or 0.2% (w/v) glucose as the only carbon source. Cell culturing was performed at 30°C with rotational shaking at 200 rpm in Erlenmeyer flasks. The "flask volume/medium volume" ratio was 5:1. Cell aliquots for separating high-density and low-density quiescent cells by centrifugation in Percoll density gradient were collected on days 1, 2, 3, 5, 7, 10, 14, 17 and 21 culturing.

2.2 Separating high- and low-density quiescent and non- quiescent cells by centrifugation in Percoll density gradient.

Using a 50-ml conical polypropylene centrifuge tube (#055398; "Fisher Scientific"), 2 ml of 1.5 M NaCl (#S7653; Sigma) and 16 ml of the Percoll solution (#P1644; "Sigma") was added to this tube, and the NaCl and Percoll solutions were mixed by pipetting. Four Percoll density gradients were pre-formed by placing 4 ml of the NaCl/Percoll mixture into each of the four ultra-clear or polyallomer tubes for an SW 55 Ti swinging-bucket rotor for a Beckman Avanti centrifuge and centrifuging at 25,000 × g for 15 min at 25°C. After taking a cell culture aliquot at a particular time-point of culturing (see section 2.1), a fraction of the aliquot was diluted and the total number of cells per ml of culture was assessed using a hemacytometer (#0267110; "Fisher Scientific"). For each Percoll density gradient, 1×10^9 yeast cells were placed into a 15-ml conical polypropylene centrifuge tube (#0553912; "Fisher Scientific"). These cells were pelleted by centrifugation at 5,000 rpm for 7 min at room temperature in a Centra CL2 clinical centrifuge ("Thermo Electron Corporation"). After resuspending the cell pellet in 500 µl of 50 mM Tris/HCl buffer (pH 7.5), the cell suspension was overlaid onto a pre-formed Percoll gradient. The gradients were centrifuged at 2,300 × g for 30 min at 25°C in an SW 55 Ti swinging-bucket rotor for a Beckman Avanti centrifuge. A pipette was used to collect the upper (low-density; volume 2 ml)

and lower (high-density; volume 2 ml) cell fractions. The cells were washed twice by centrifugation at 16,000 × g for 1 min at room temperature (RT) in 50 mM Tris/HCl buffer (pH 7.5) to remove Percoll. The cell pellets after the second wash were resuspended in 50 mM Tris/HCl buffer (pH 7.5) for further analysis.

2.3 Assessing the percentage of high-density cells.

The upper (low-density) and lower (high-density) cell fractions were collected using a pipette, as described in section 2.2. The cell suspension of each cell fraction was centrifuged at 16,000 × g for 1 min at RT. After discarding the supernatant, the cell pellet of each cell fraction was resuspended in 1 ml of 50 mM Tris/HCl buffer (pH 7.5). Ten-fold serial dilutions of a fraction of each cell suspension were made. The total number of cells per ml of the upper (low-density) and lower (high-density) cell fractions was measured using a hemacytometer (#0267110; "Fisher Scientific"). These cell counts were used to calculate the percentages of high-density cells for WT and mutant cell cultures recovered at a particular time-point.

2.4 Measuring diameters of high- and low-density cells.

The upper (low-density) and lower (high-density) cell fractions were collected using a pipette, as described in section 2.2. The cell suspension of each cell fraction was centrifuged at 16,000 × g for 1 min at RT. After discarding the supernatant, the cell pellet of each cell fraction was resuspended in 1 ml of 50 mM Tris/HCl buffer (pH 7.5). After making ten-fold serial dilutions of a fraction of each cell suspension as described in section 2.3, the remaining portion of each cell suspension was centrifuged at 16,000 × g for 1 min at RT, and the supernatant was discarded. The pellet was resuspended in the volume of 50 mM Tris/HCl buffer (pH 7.5), which was sufficient to give the final cell titer at ~1 × 10^9 cells/ml. For each sample, the cell diameters were calculated as follows: images of yeast cells were captured using a Leica DMI6000 microscope equipped with DIC optics, 100× Plan Fluotar lens (NA1.4) and a Hamamatsu Orca ER camera using Volocity software. Using FIJI's "fit ellipse" tool, cell diameters were calculated after identifying the yeast cells using the YeastSpotter neural net (Lu et al., 2019; He et al., 2018). Only the cells whose circularity values exceed 0.9 were analyzed; A value of 1.0 indicates a perfect circle. Cell diameter was calculated using the following equation: Cell Diameter (μm) = $2\sqrt{\text{Cell Area } (\mu m^2)/\pi}$.

2.5 Reproductive (colony-forming) capability assay for high- and low-density cells separated by centrifugation in Percoll density gradient.

A high- or low-density cell fraction was recovered from the Percoll density gradient, as described in section 2.2. The cells were washed twice by centrifugation in 50 mM Tris/HCl buffer (pH 7.5) to remove Percoll. An aliquot of the washed high- or low-density cell fraction was diluted. The total number of cells per ml of cell suspension was measured using a hemacytometer (#0267110; "Fisher Scientific"). Serial dilutions ($1:10^2$ to $1:10^6$) of cells were made and plated onto in the solid nutrient-rich YP medium (1% (w/v) yeast extract and 2% (w/v) peptone; both from "Fisher Scientific") supplemented with 2% (w/v) glucose ("Fisher Scientific") as the only carbon source. Then, 100 µl of the washed and diluted high- or low-density cell fraction was plated onto each plate. The plates were incubated for 48 h at 30°C, and the number of colonies per plate was counted. The number of colony-forming units (CFU) equals the number of reproductively capable cells in a sample (i.e., 100 µl). Thus, the number of reproductively capable cells was calculated as follows: the number of CFU × dilution factor × 10 = the number of reproductively capable cells per ml. For each cell fraction assayed, the % reproductive capability of the cells was calculated as follows: number of CFU per ml/total number of cells per ml × 100%.

2.6 Chronological lifespan measurement.

A 1 mL sample of cell culture was taken from a liquid culture at a particular time point. Ten-fold serial dilutions of a fraction of the cell culture sample were made. A hemacytometer (#0267110; Fisher Scientific) was used to measure the number of cells per mL of cell suspension. Ten-fold serial dilutions of another fraction of the cell culture sample were made. A total volume of 100 µl of each of these serial dilutions was plated in duplicate onto YP plates supplemented with 2% (w/v) glucose ("Fisher Scientific") as the only carbon source. The plates were incubated for 48 h at 30°C, and the number of colonies per plate (i.e., cell number per 100 µl of cell culture) was counted. The percentage of viable cells for each culture was calculated as follows: (number of viable cells per ml/total number of cells per ml) × 100. The percentage of viable cells in the mid-logarithmic growth phase was set at 100%.

2.7 Statistical analysis.

The Microsoft Excel's (2010) Analysis ToolPak – VBA was used to perform statistical analysis. All data are provided as mean ± SD. The GraphPad Prism 7 statistics software was used to calculate the *p* values for comparing the means of two groups using an unpaired two-tailed *t* test.

Chapter 3: Results

3.1 CR, *tor1Δ* and *sch9Δ* mutations differently regulate process 1 integrated into the cellular quiescence program.

My first hypothesis posits that CR arrests the cell cycle in early G_1 and creates small Q^{HD} cells. Additionally, similar to CR, *tor1Δ* and *sch9Δ* mutant cell lines may also arrest the cell cycle in early G_1 and make small Q^{HD} because these mutations are part of the pro-longevity TORC-Sch9 nutrient signaling branch whose downstream processes are integrated into the cellular quiescence program. Previous studies have shown that in WT yeast cultured under non-CR, process 1 occurs at the checkpoint "START A" in late G_1 and results in the formation of large-sized (cell diameter ~ 4.5-5.0 μm) Q^{HD} cells (Allen et al., 2006; Werner-Washburne et al., 2012; Leonov et al., 2017). Whereas, in WT yeast cultured under CR, process 1 occurs at a different checkpoint in the early G1 phase, resulting in small-sized Q^{HD} cells (cell diameter ~ 3.0-3.5 μm) (Leonov et al., 2017). Therefore, to investigate whether CR, *tor1Δ* and *sch9Δ* similarly regulate process 1, I used centrifugation in Percoll density gradient to purify the Q^{HD} and Q^{LD} cell populations from WT non-CR, WT under CR, *tor1Δ* mutant under non-CR, and *sch9Δ* mutant under non-CR. Samples of cells were recovered at different days following glucose exhaustion, which occurs 16 or 22 h after cell inoculation, respectively (Figure 3.1; Leonov et al., 2017). The purified Q^{HD} and Q^{LD} cell populations were then subjected to the differential interference contrast (DIC) microscopical examination to assess the size and morphology of the cells comprising these populations and evaluate each population's homogeneity (Figures 6.1-6.8 in Supplemental Data).

I found that in yeast cultures of different chronological ages, the Q^{HD} and Q^{LD} cells remain mostly unbudded (especially the Q^{HD} cells) and similarly sized (cell diameter 4.0-4.8 μm) in WT and *tor1Δ* cells (Figures 3.2A, 3.3A; 6.1, 6.3, 6.5, 6.7 in Supplemental Data). This finding indicates that akin to WT yeast cultured under non-CR (Allen et al., 2006; Werner-Washburne et al., 2012; Leonov et al., 2017), process 1 in *tor1Δ* cells happens at the checkpoint "START A" in late G_1 and results in the formation of large-sized (cell diameter 4.3-4.8 μm) Q^{HD} cells. Furthermore, because

the sizes of Q^{HD} and Q^{LD} cells in WT and the QHD and QLD cells in tor1Δ cultures remained similar, I concluded that the QHD-to-Q^{LD} conversion in these cultures does not involve the change in the checkpoint at which the cell cycle is arrested before the conversion. Therefore, the Q^{HD} and Q^{LD} cells in WT and *tor1Δ* cultures do not change their sizes significantly during the Q^{HD}-to-Q^{LD} conversion because they do not change the position at which they arrest their cell cycle in late G1.

The morphometric analysis also revealed that Q^{HD} cells are commonly unbudded and considerably smaller (cell diameter 3.2-3.5 μm) in differently aged cultures of WT yeast under CR than they are in WT or *tor1Δ* yeast cultured under non-CR (cell diameter 4.3-4.8 μm) (compare Figure 3.2A; Figures 6.1 and 6.2 in Supplemental Data). This finding was in line with expectations that CR arrests the cell cycle and causes entry into the G_0 state of quiescence at a checkpoint in early G_1 (Leonov et al., 2017). Moreover, I found that Q^{LD} cells in WT yeast cultured under CR conditions are almost universally unbudded and have sizes (cell diameter 3.8-4.0 μm) similar to Q^{LD} cells in WT and *tor1Δ* cultures under non-CR (cell diameter 4.0-4.8 μm) (compare Figures 3.2A and 3.3A; compare Figure 6.6 to Figures 6.5 and 6.7 in Supplemental Data). It needs to be emphasized that the diameter of Q^{LD} cells in WT cultures under CR (cell diameter 3.8-4.0 μm) exceeded the diameter of Q^{HD} cells in these cultures (cell diameter 3.2-3.5 μm). The diameter of Q^{LD} cells in WT cultures under CR (cell diameter 3.8-4.0 μm) was similar to those of Q^{HD} cells in WT and *tor1Δ* cultures under non-CR (cell diameter 4.0-4.8 μm). Based on these observations, I concluded that WT cells cultured under CR arrest their cell cycle in early G_1, crate small Q^{HD} cells. Additionally, during the Q^{HD}-to-Q^{LD} conversion, the checkpoint is shifted from early G_1 to "START A" in late G_1 (i.e., Q^{HD} cells enlarged during this conversion).

The morphometric analysis showed that neither Q^{HD} nor Q^{LD} cell populations purified from *sch9Δ* cultures under non-CR and recovered from different phases of culturing are homogenous in terms of the sizes of cells comprising them (Figures 3.2A and 3.3A; compare Figures 6.4 and 6.8 in Supplemental Data). Specifically, two groups of cells were present in the Q^{HD} and Q^{LD} cell populations from *sch9Δ* cultures under non-CR. I call them group 1 (cell diameter 3.2-3.3 μm in the Q^{HD} population and 2.7-3.0 μm in the Q^{LD} population) and group 2 (cell diameter 4.2-4.3 μm in the Q^{HD} population and 4.4-5.0 μm in the Q^{LD} population) cells (Figures 6.3 and 6.4 in Supplemental Data). The sizes of Q^{HD} cells in WT cultures under CR were similar to group 1 Q^{HD} cells in *sch9Δ* cultures under non-CR (3.2-3.5 μm and 3.2-3.3 μm, respectively). Additionally, the sizes of Q^{HD} and Q^{LD} cells in WT and *tor1Δ* cultures under non-CR were similar to those of group 2 Q^{HD} and Q^{LD} cells in *sch9Δ* cultures under non-CR (4.0-4.8 μm and 4.2-5.0, respectively). The

above findings on Q^{HD} and Q^{LD} cells in *sch9Δ* cultures suggest that process 1 of cell cycle arrest occurs at two different cell cycle checkpoints where some *sch9Δ* cells arrest the cell cycle in late G_1, while others arrest their cell cycle in early G_1. These findings suggest that the Q^{HD}-to-Q^{LD} conversion in *sch9Δ* cultures under non-CR does not involve changes in the checkpoint at which the cell cycle is arrested before the conversion. Thus, the Q^{HD} and Q^{LD} cells in *sch9Δ* cultures under non-CR conditions do not change their sizes substantially during the Q^{HD}-to-Q^{LD} conversion because they do not change the position at which they arrest their cell cycle in either early G_1 (Group 1) or late G_1 phase (Group 2).

In sum, the data presented in section 3.1 suggest that CR, *tor1Δ* and *sch9Δ* slow the CLS of *S. cerevisiae* because each of them arrests the cell cycle, trigger entry into the G_0 state of quiescence, and causes the formation of the Q^{HD} cells at the different checkpoints of the cell cycle. In all WT cells under non-CR (Leonov et al., 2017), all *tor1Δ* cells under non-CR, and in some *sch9Δ* cells under non-CR arrest their cell cycle at the checkpoint "START A" in late G_1 and lead to the formation of large-sized Q^{HD} cells (cell diameter 4.3-4.8 μm) (Figure 3.2B). In all WT yeast under CR (Leonov et al., 2017) and some *sch9Δ* cells under non-CR, process 1 takes place at a different checkpoint in the early G_1 phase and yields small-sized Q^{HD} cells (cell diameter 3.2-3.5 μm) (Figure 3.2B).

The data presented in section 3.1 also indicate that the Q^{HD}-to-Q^{LD} conversion in most cultures happens when the cell cycle is arrested at the checkpoint "START A" in late G_1. The cultures include all WT cells under CR and non-CR (Leonov et al., 2017), *tor1Δ* cells under non-CR, and some *sch9Δ* cells under non-CR (specifically, the ones whose cell cycle has been arrested at the checkpoint "START A" in late G_1; Only in those *sch9Δ* cells whose cell cycle has been arrested, and the quiescent state has been entered at a checkpoint in early G_1, the Q^{HD}-to-Q^{LD} conversion occurs when the cell cycle is arrested at this specific checkpoint.

The cell cycle arrest, entry into the G_0 state of quiescence, and formation of differently-sized Q^{HD} cells somehow enhance the pro-longevity properties of these Q cells. A challenge for the future is understanding how the enhancement of the Q cells' pro-longevity properties is linked to the cell cycle arrest at the early or late G_1 checkpoints.

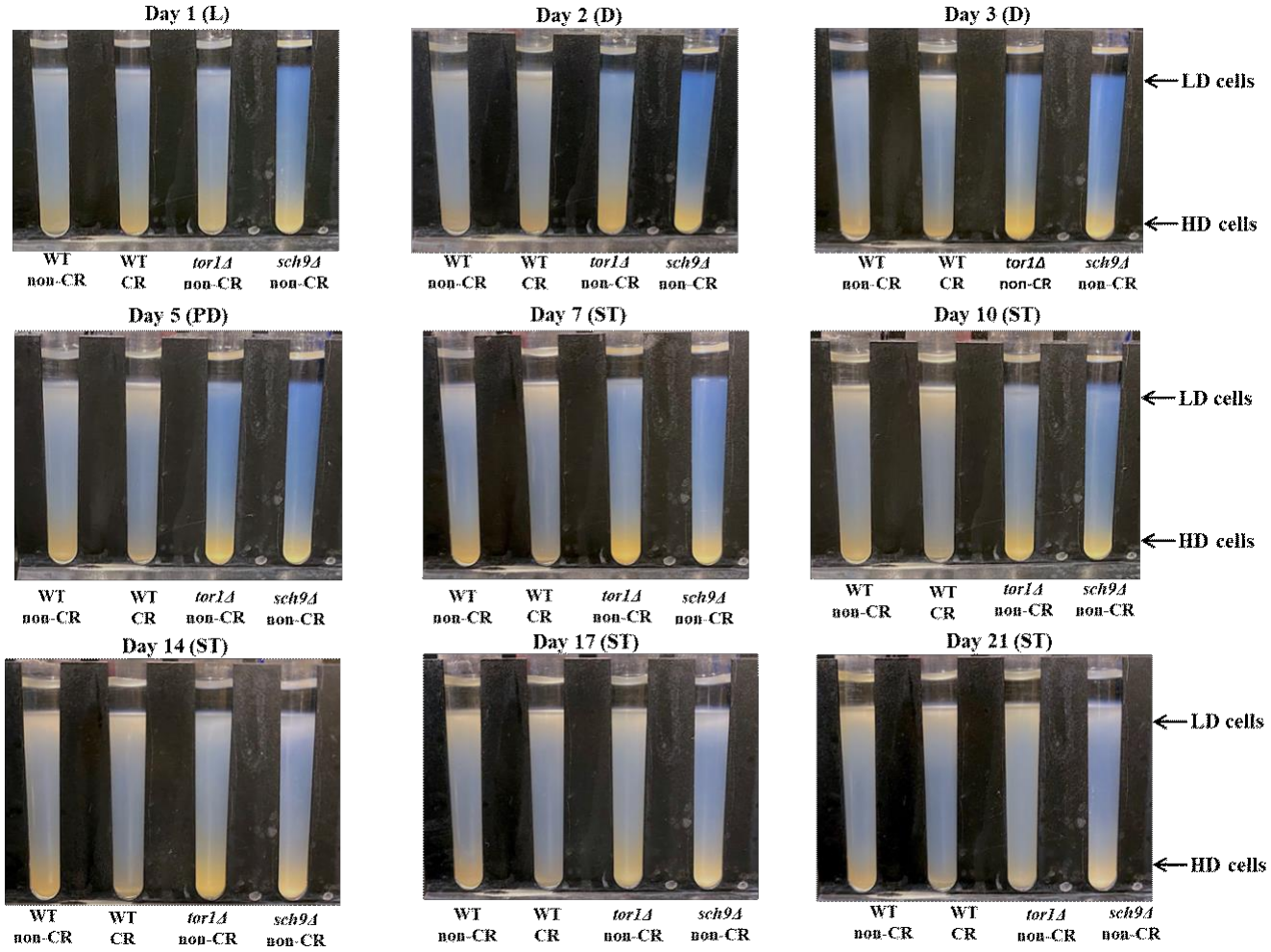

Figure 3.1: Purification of the Q^{HD} and Q^{LD} cell populations from WT and mutant yeast by centrifugation in Percoll density gradient. Samples of WT, *tor1Δ* and *sch9Δ* yeast cultured in the nutrient-rich YP medium initially containing 0.2% glucose (CR) or 2% glucose (non-CR) were recovered from logarithmic (L), diauxic (D), post-diauxic (PD) or stationary (ST) phase of culturing. These samples were then subjected to centrifugation in Percoll density gradient. Other abbreviations: HD, high-density cells; LD, low-density cells; Q, quiescent cells.

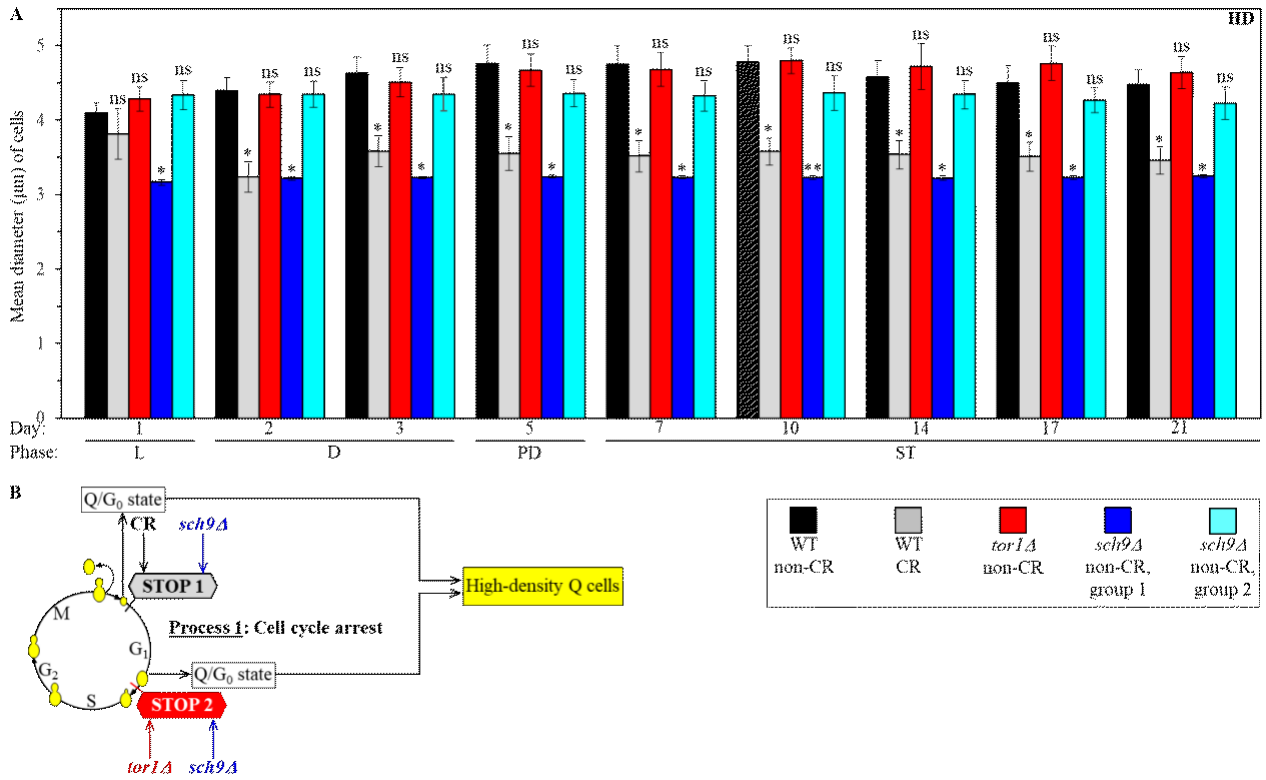

Figure 3.2: The sizes (mean diameters ± SD) of Q^{HD} cell populations. These populations were purified from WT or mutant cells cultured under CR or non-CR, recovered from different phases of culturing, subjected to DIC and comparative morphometric analysis. **(A)** WT and mutant yeast cultured in the nutrient-rich YP medium initially containing 2% glucose (non-CR) or 0.2% glucose (CR). Cell aliquots were recovered on different days of culturing. These aliquots were then subjected to centrifugation in a Percoll density gradient. The Q^{HD} cell populations were retrieved, subjected to the DIC and analyzed morphometrically. **(B)** The CR, *tor1Δ* and *sch9Δ* mutations arrest the cell cycle, trigger entry into the G_0 state of quiescence and cause the formation of the Q^{HD} cells at the different checkpoints of the cell cycle. In all *tor1Δ* and some *sch9Δ* cells under non-CR, these events occur at the checkpoint "START A" in late G_1 and form large-sized (cell diameter 4.2-4.8 µm) Q^{HD} cells. In some *sch9Δ* cells under non-CR, cell cycle arrest occurs at a different checkpoint in the early G_1 phase and yields small-sized (cell diameter 3.2-3.5 µm) Q^{HD} cells (Figure 3.2B). An unpaired *t*-test was used to verify the significance between each culture compared to the WT non-CR. Data are presented as means ± SEM ($n = 3$; *$p < 0.05$; **$p < 0.01$; ***p < 0.001; ns, not significant). Abbreviations: DIC, Abbreviation: DIC, differential interference contrast; Q^{HD}, high-density quiescent cells.

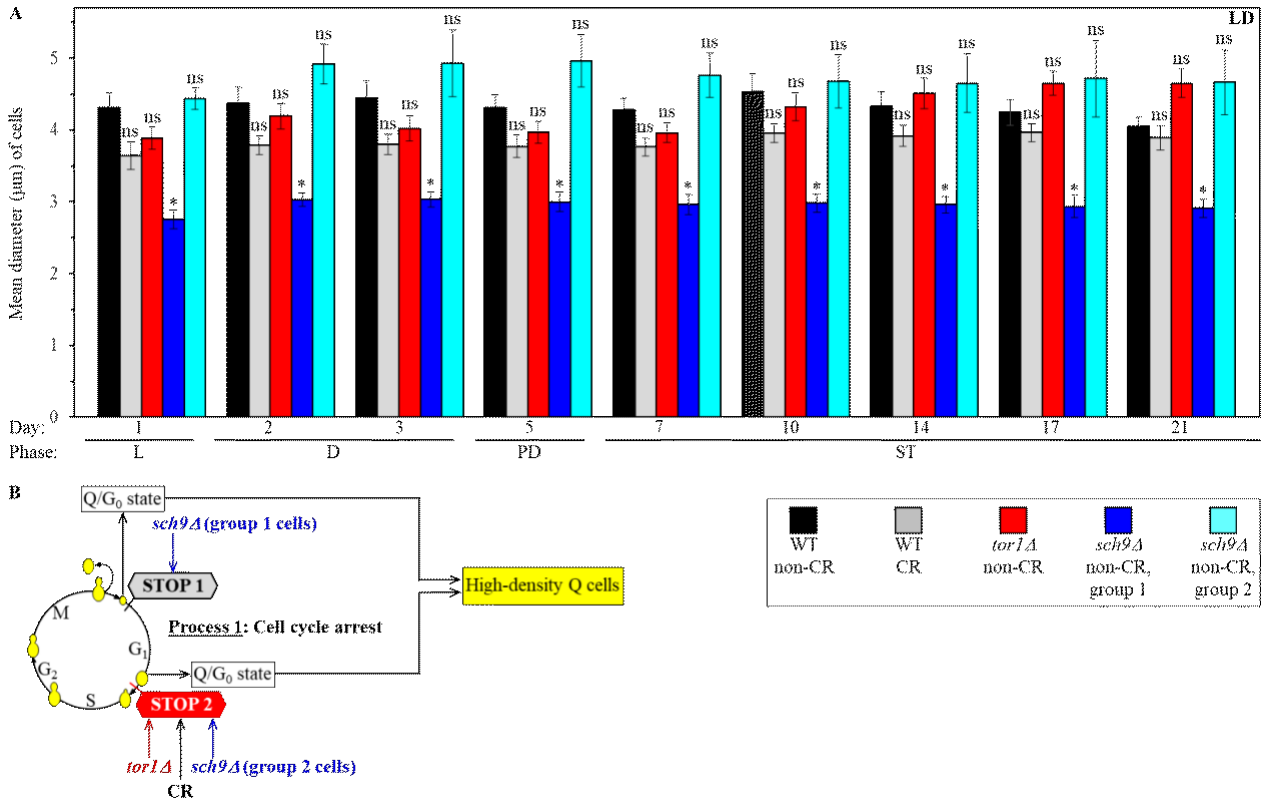

Figure 3.3: The sizes (mean diameters ± SD) of Q^{LD} cell populations. These populations were purified from WT or mutant cells cultured under CR or non-CR, recovered from different phases of culturing, subjected to DIC and comparative morphometric analysis. **(A)** WT and mutant yeast cultured in the nutrient-rich YP medium initially containing 2% glucose (non-CR) or 0.2% glucose (CR). Cell aliquots were recovered on different days of culturing. These aliquots were then subjected to centrifugation in a Percoll density gradient. The Q^{LD} cell populations were retrieved, subjected to the DIC and analyzed morphometrically. **(B)** The Q^{HD}-to-Q^{LD} conversion in most cultures happens when the cell cycle is arrested at the checkpoint "START A" in late G_1. The cultures include all WT cells under CR, all *tor1Δ* cells and some *sch9Δ* cells (specifically, those whose cell cycle has been arrested at the checkpoint "START A" in late G_1). Only in those *sch9Δ* cells whose cell cycle has been arrested and the quiescent state has been entered at a checkpoint in early G_1, the Q^{HD}-to-Q^{LD} conversion occurs when the cell cycle is arrested at this specific checkpoint. An unpaired *t*-test was used to verify the significance between each culture compared to the WT non-CR. Data are presented as means ± SEM (n = 3; *$p < 0.05$; **$p < 0.01$; ***p < 0.001; ns, not significant). Abbreviations: DIC, Abbreviation: DIC, differential interference contrast; Q^{LD}, low-density quiescent cells.

3.2 CR, *tor1Δ* and *sch9Δ* regulate process 2 of the cellular quiescence program differently.

Based on the early observation of process 2 acceleration under CR, it is hypothesized that the promoted Q^{HD}-to-Q^{LD} cell conversion somehow improves some or all pro-longevity properties of Q cells indicated in Figure 1.5 (Leonov et al., 2017). I hypothesized that the phenotype of the *tor1Δ* and *sch9Δ* mutations are also geroprotective via process 2 of the cellular quiescence program by promoting the Q^{HD}-to-Q^{LD} cell conversion, similarly to CR. Therefore, using Percoll density gradient purification of the cell populations, the percentage of Q^{HD} cells was determined to assess the extent of Q^{LD} cell accumulation during the Q^{HD}-to-Q^{LD} cell conversion of process 2.

I found that chronologically aging cultures of WT yeast under CR and non-CR contain both LD and HD cells throughout the whole chronological lifespan, namely during logarithmic (L), diauxic (D), post-diauxic (PD) and stationary (ST) phases of culturing (Figure 3.1). The percentage of LD cells in both WT cultures increased throughout the whole chronological lifespan, although much faster under CR (compare the first and second Percoll density gradient tubes in Figure 3.1). In contrast, the *tor1Δ* and *sch9Δ* mutant yeast cultured under non-CR revealed that the percentage of LD cells in both the mutant cultures increased on day 14, i.e., late in the chronological lifespan (compare the third and fourth Percoll density gradient tubes to the first and second tubes in Figure 3.1). This visual assessment of WT, WT under CR, *tor1Δ* and *sch9Δ* mutant yeast cells was further confirmed by quantitative analysis.

CR was shown to accelerates process 2 of an age-related conversion of the Q^{HD} cells into Q^{LD} cells, as expected (Leonov et al. 2017). The percentage of Q^{HD} cells substantially lowers as early as day 2 of culturing, suggesting a progressive conversion of Q^{HD}-to-Q^{LD} cells (Figures 3.1 and 3.4). Unlike CR, the *tor1Δ* and *sch9Δ* mutations substantially slowed down the Q^{HD}-to-Q^{LD} cell conversion. This can be seen by the high percentage of the Q^{HD} cells throughout the CLS (Figures 3.1 and 3.4). Because the *tor1Δ* and *sch9Δ* mutants are long-lived, these findings suggest that there are at least two ways of enhancing some or all of the pro-longevity properties of Q cells by either accelerating or decelerating the pace of Q^{HD}-to-Q^{LD} cell conversion.

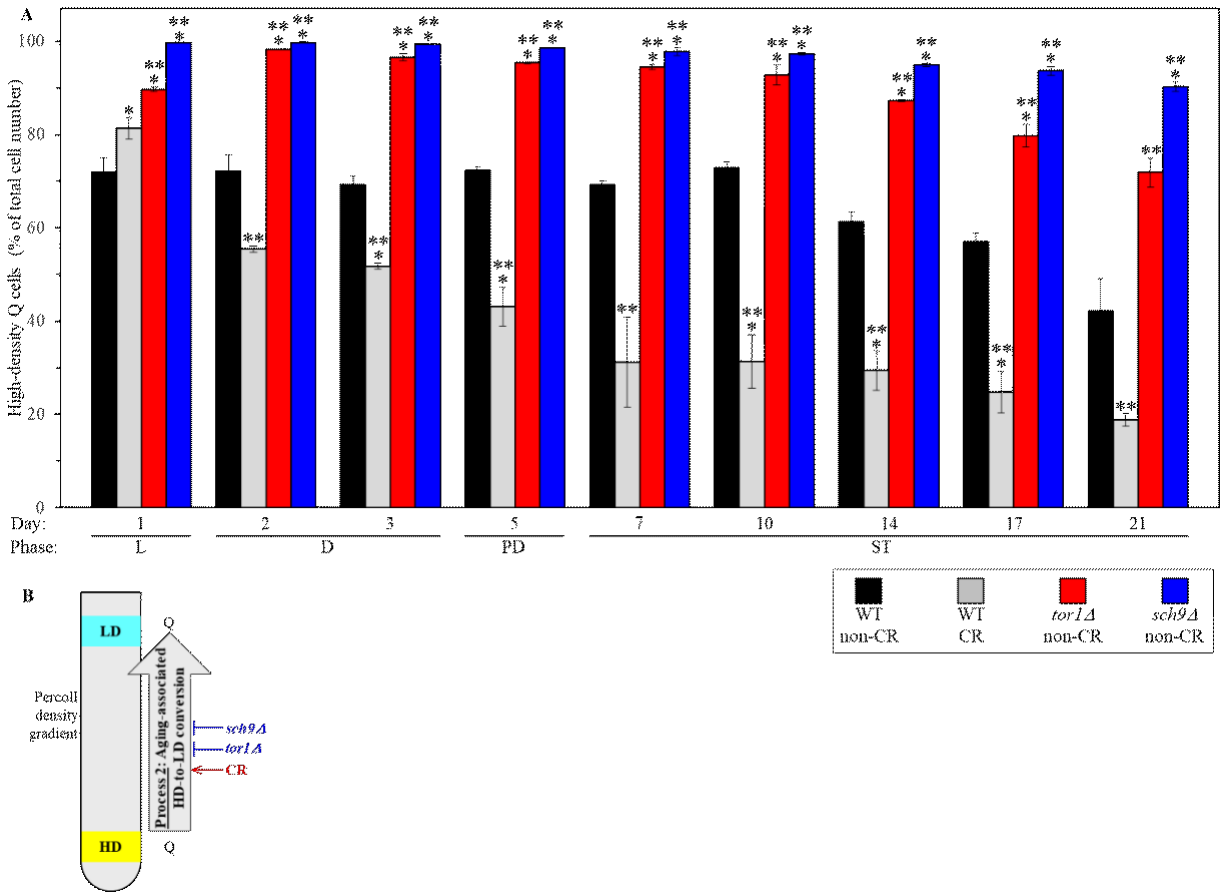

Figure 3.4: CR accelerates process 2 of an age-related conversion of the Q^{HD} cells into Q^{LD} cells. In contrast, the *tor1Δ* and *sch9Δ* mutations (both under non-CR) substantially slow down process 2 of the Q^{HD}-to-Q^{LD} cell conversion. **(A)** WT and mutant yeast cultured in the nutrient-rich YP medium initially containing 2% glucose (non-CR conditions) or 0.2% glucose (CR conditions). Cell aliquots were recovered on different days of culturing. These aliquots were then subjected to centrifugation in a Percoll density gradient. The percentage of high-density Q cells was measured as described in the Materials and Methods chapter of the Thesis. **(B)** CR accelerates process 2 of an age-related conversion of the Q^{HD} cells into Q^{LD} cells, whereas the *tor1Δ* and *sch9Δ* mutations (both under non-CR) decelerate this process. An unpaired t-test was used to verify significance between each culture compared to the WT non-CR. Data are presented as means ± SEM ($n = 3$; *$p <$ 0.05; **$p < 0.01$; ***p < 0.001; ns, not significant).

3.3 CR, *tor1Δ* and *sch9Δ* decelerate processes 3 and 4 of the aging-associated fast and slow declines in the clonogenicities of the Q^{LD} and Q^{HD} cells, respectively.

Clonogenicity is defined as the ability of a cell to form a colony after it is taken from a nutrient-depleted liquid medium and plated on the surfaces of Petri dishes with a solid nutrient-rich medium. Clonogenicity is the most distinguishing property of the Q cells because NQ cells are significantly less viable (Allen et al., 2006; Aragon et al., 2008; Davidson et al., 2011; Werner-Washburne et al., 2012; Miles et al., 2013; Leonov et al., 2017). CR slows the conversion of the Q^{LD} cells into NQ^{LD} cells (Figure 1.5, process 3); This aging-associated process 3 of quiescence decline is fast. CR also decelerates a transformation of the Q^{HD} cells into NQ^{HD} cells (Figure 1.5, process 4); This aging-associated process of quiescence decline is slow (Leonov et al., 2017)

Based on these observations, I hypothesized that CR, *tor1Δ* and *sch9Δ* mutations similarly decelerate processes 3 and 4 of the aging-associated fast and slow declines in the clonogenicities of the Q^{LD} and Q^{HD} cells respectively. These processes' decelerations somehow contribute to the acquisition by the Q^{LD} and Q^{HD} cells of some or all pro-longevity properties named in Figure 1.5. Using Percoll density gradient centrifugation, the purified Q^{HD} and Q^{LD} cell populations were subjected to the clonogenic plating assay. I investigated how CR and the tor1Δ and sch9Δ mutations influence the pace of aging-associated fast and slow declines in the clonogenicities of the Q^{LD} and Q^{HD} cells.

As expected, CR was shown to decelerate processes 3 and 4 (Leonov et al., 2017). The WT Q^{LD} and Q^{HD} cells under non-CR exhibited low viability as early as day 2 of culturing, whereas Q^{LD} and Q^{HD} CR cells maintained high clonogenicity until day 5 (Figures 3.5 and 3.6). Akin to CR, the *tor1Δ* and *sch9Δ* mutant phenotypes considerably slowed down processes 3 and 4 by maintaining high viability until day 5 (Figures 3.5 and 3.6). These findings confirm that the CR- and *tor1Δ* and *sch9Δ* mutations decelerate the rate of Q^{LD}-to-NQ^{LD} and Q^{HD}-to-NQ^{HD} cell conversions, contributing to the maintenance of pro-longevity Q properties that extend the CLS.

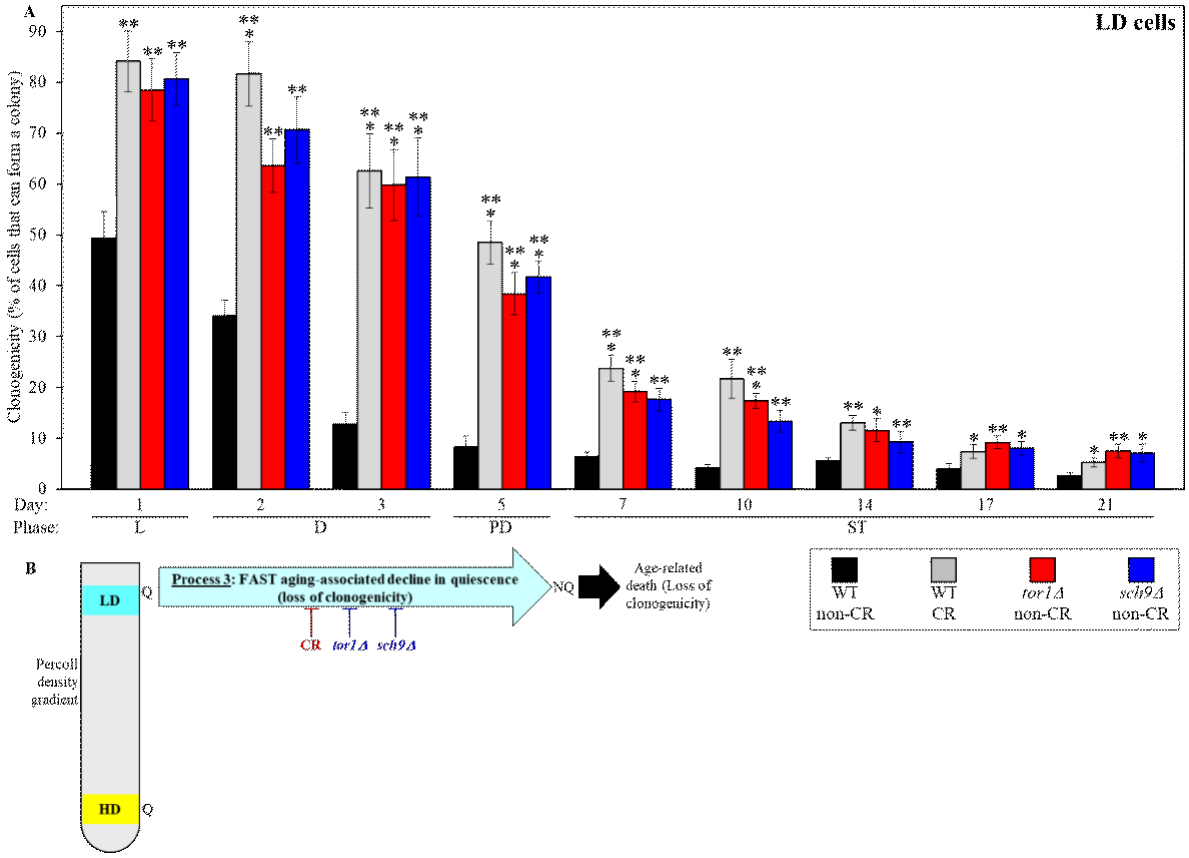

Figure 3.5: CR, *tor1Δ* and *sch9Δ* decelerate process 3 of the aging-associated fast decline in the clonogenicity of the Q^{LD} cells. **(A)** WT and mutant yeast cultured in the nutrient-rich YP medium initially containing 2% glucose (non-CR) or 0.2% glucose (CR). Cell aliquots were recovered on different days of culturing. These aliquots were then subjected to centrifugation in a Percoll density gradient. The purified Q^{LD} cell fraction was subjected to a reproductive (colony-forming) capability assay to measure the clonogenicity of these cells. **(B)** A model for how CR, *tor1Δ* (non-CR) and *sch9Δ* (non-CR) affect an aging-associated deterioration in the clonogenicities of Q^{LD} cells during process 3 of the cellular quiescence program. An unpaired *t*-test was used to verify the significance between each culture compared to the WT non-CR. Data are presented as means ± SEM ($n = 3$; *$p < 0.05$; **$p < 0.01$; ***p < 0.001; ns, not significant). Other abbreviations: LD, low-density cells; Q, quiescent cells; NQ, non-quiescent cells.

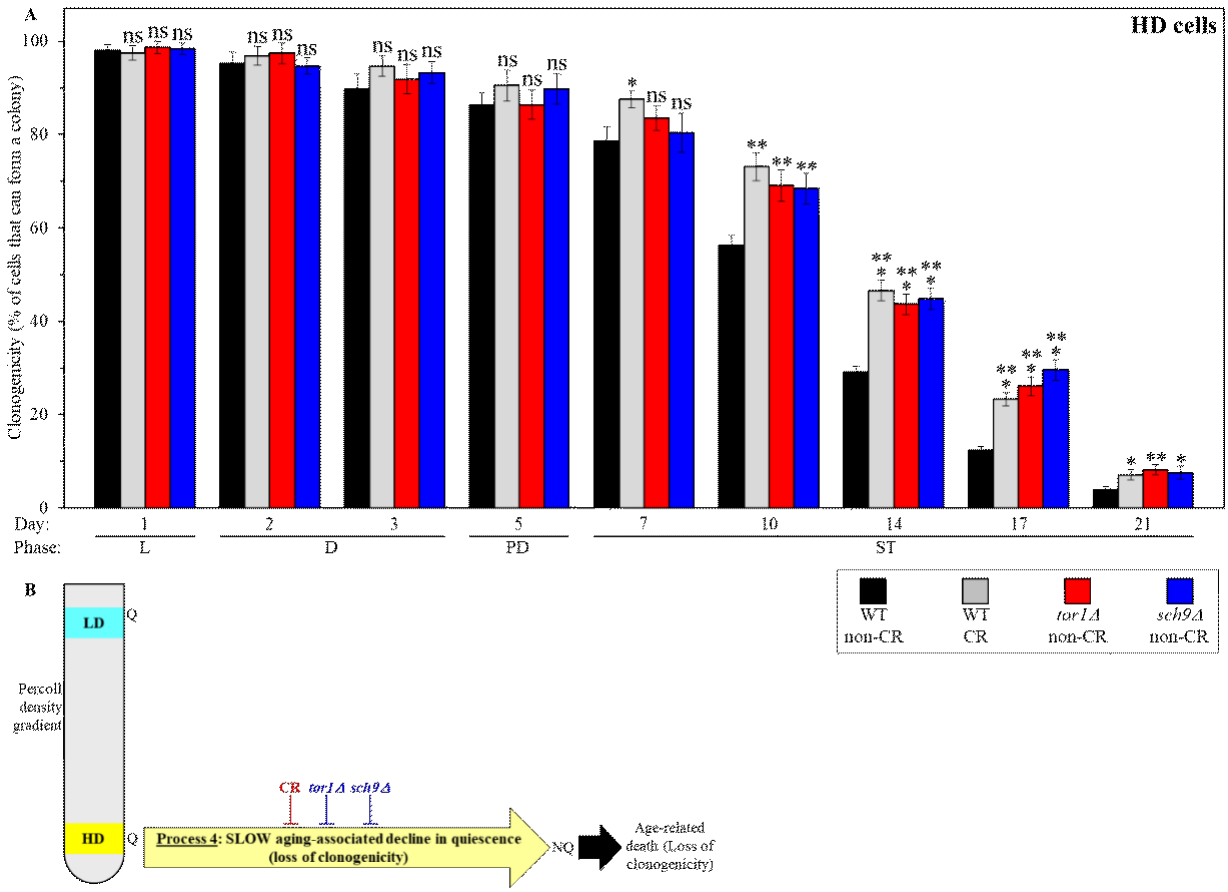

Figure 3.6: CR, *tor1Δ* and *sch9Δ* decelerate process 4 of the aging-associated fast decline in the clonogenicity of the Q^{HD} cells. **(A)** WT and mutant yeast cultured in the nutrient-rich YP medium initially containing 2% glucose (non-CR) or 0.2% glucose (CR). Cell aliquots were recovered on different days of culturing. These aliquots were then subjected to centrifugation in a Percoll density gradient. The purified Q^{HD} cell fraction was subjected to a reproductive (colony-forming) capability assay to measure the clonogenicity of these cells. **(B)** A model for how CR, *tor1Δ* (non-CR) and *sch9Δ* (non-CR) affect an aging-associated deterioration in the clonogenicities of Q^{HD} cells during process 4 of the cellular quiescence program. An unpaired *t*-test was used to verify significance between each culture compared to the WT non-CR. Data are presented as means ± SEM ($n = 3$; *$p < 0.05$; **$p < 0.01$; ***p < 0.001; ns, not significant).Other abbreviations: LD, low-density cells; Q, quiescent cells; NQ, non-quiescent cells.

Chapter 4: Discussion

This study and previously published data suggest a link between chronological aging and cellular quiescence in *S. cerevisiae* (Leonov et al., 2017). One important finding presented is that the dietary intervention, CR, and the two genetic interventions, *tor1Δ* and *sch9Δ* mutations, affect all four processes converged into the mechanism linking chronological aging to cellular quiescence. The other important finding is that CR and *tor1Δ* and *sch9Δ* mutations exhibit robust geroprotective effects despite differently regulating processes 1 and 2 of cell quiescence.

CR (in all cells) and the *sch9Δ* mutant phenotype (in some cells) decelerated chronological aging because they both stimulated the development of the Q^{HD} cells (process 1) by arresting the cell cycle in early G_1. Yet, the *tor1Δ* mutation and the *sch9Δ* mutation (in some cells) delay yeast chronological aging because they both promoted the development of the Q^{HD} cells by arresting the cell cycle in late G_1. Additionally, CR promoted the aging-associated Q^{HD}-to-Q^{LD} cell conversion (process 2), while the *tor1Δ* and the *sch9Δ* mutation displayed a decelerated phenotype of this conversion. Therefore, all three interventions demonstrated geroprotective effects by differently regulating processes 1 and 2. This can be seen by the delay of the fast aging-associated deterioration in clonogenicity of the Q^{LD} cells (process 3) and the postponement of the slow aging-associated decline in clonogenicity of Q^{HD} cells (process 4).

It needs to be emphasized that all three interventions tested exhibit a common ability to postpone processes 3 and 4 of the quiescence program. Such a common ability provides strong support for the existence of a mechanism that links chronological aging to cellular quiescence. Indeed, the ability to postpone clonogenic deterioration by Q cells might contribute to the delay of yeast chronological aging because it allows Q cells to maintain a pro-longevity cellular pattern longer than Q cells in untreated cultures. These pro-longevity cellular patterns of Q cells include an enhanced reproductive competence, an increase in glycogen and trehalose concentrations, a decrease in the concentrations of TAG, a rise in CL concentrations, a decline in the concentrations of ROS, an improvement of mitochondrial functionality, lowered oxidative damage to macromolecules, a rise in cell resistance to long-term thermal and oxidative stresses, and a deterioration in cell susceptibility to apoptotic and liponecrotic forms of regulated cell death (Figure 1.5; Leonov et al., 2017). Thus, CR and the *tor1Δ* and the *sch9Δ* phenotypes suggest that nutrients' limitations affect the core protein hubs of the nutrient-signaling pathways by activating

or inactivating specific downstream processes involved in organismal fitness. One may speculate that the entry and maintenance of Q is an essential evolutionary conserved mechanism that enables organisms to survive periods of scarcity in their natural environments.

A challenge for the future is to learn how differently diverse geroprotectors and geroprotective phenotypes of mutations inferred in other core hub nutrient-sensing pathways affect the processes of the quiescence program. One possibility is that differently regulating processes 1 and 2 does not delay the chronological lifespan of *S. cerevisiae*. An alternative opportunity is that there are two different ways of employing changes in processes 1 and 2 to decelerate the chronological clock. Also, further research is needed to address the nature of the pro-longevity Q properties and how their enhancement is related to cell cycle arrest.

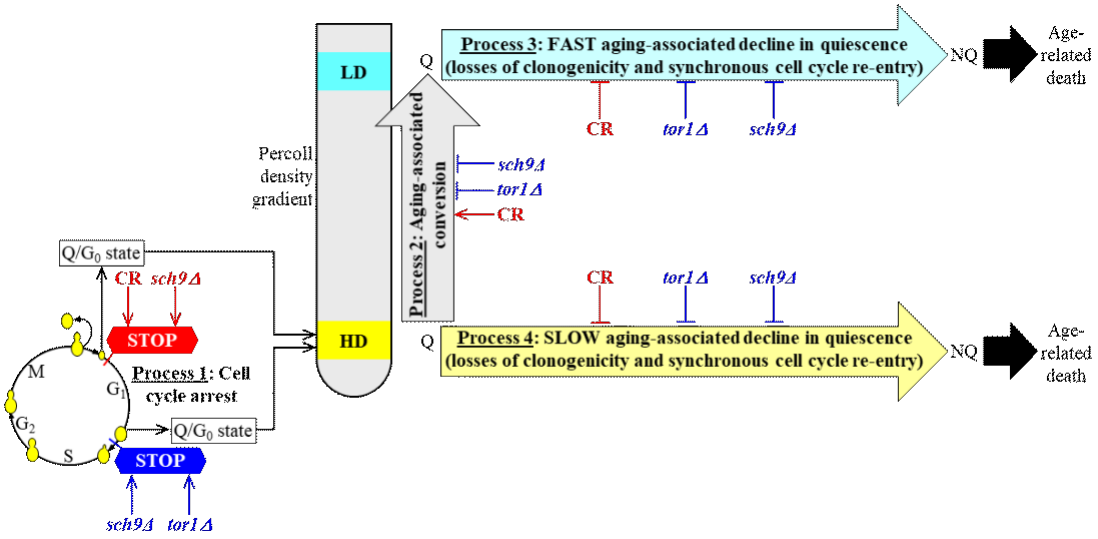

Figure 4.1: A model demonstrating how CR, *tor1Δ* and *sch9Δ* delay yeast chronological aging by affecting the quiescence mechanisms differently. The first way is to initiate the formation of the Q^{HD} cells (process 1) by arresting the cell cycle in early G_1, speed up an aging-associated conversion of the Q^{HD} cells into Q^{LD} cells (process 2), slow down a fast aging-associated decline in clonogenicity of the Q^{LD} cells (process 3) and decelerate a slow aging-associated decline in clonogenicity of the Q^{LD} cells (process 4). CR (in all cells) and the *sch9Δ* mutation (in some cells) postpone yeast chronological aging because they operate via the first way. The second way is to promote the development of the Q^{HD} cells (process 1) by arresting the cell cycle in late G_1, postpone the aging Q^{HD}-to-Q^{LD} cell conversion (process 2), delay a fast aging-associated decline in clonogenicity of low-density Q^{LD} cells (process 3) and decelerate a slow aging-associated decline in clonogenicity of the Q^{HD} cells (process 4). The *tor1Δ* mutation and the *sch9Δ* mutation (in some cells) delay yeast chronological aging because they act via the second way of targeting the mechanism potentially linking chronological aging to cellular quiescence. Abbreviations: HD, high-density cells; LD, low-density cells; Q, quiescent cells.

Chapter 5: References

Allen C, Büttner S, Aragon AD, Thomas JA, Meirelles O, Jaetao JE, Benn D, Ruby SW, Veenhuis M, Madeo F, Werner-Washburne M. Isolation of quiescent and non-quiescent cells from yeast stationary-phase cultures. J Cell Biol. 2006; 174:89-100.

Aragon AD, Rodriguez AL, Meirelles O, Roy S, Davidson GS, Tapia PH, Allen C, Joe R, Benn D, Werner-Washburne M. Characterization of differentiated quiescent and non-quiescent cells in yeast stationary-phase cultures. Mol Biol Cell. 2008; 19:1271-1280.

Arlia-Ciommo A, Leonov A, Piano A, Svistkova V, Titorenko VI. Cell-autonomous mechanisms of chronological aging in the yeast Saccharomyces cerevisiae. Microb Cell. 2014; 1:163-178.

Beach A, Richard VR, Bourque S, Boukh-Viner T, Kyryakov P, Gomez-Perez A, Arlia-Ciommo A, Feldman R, Leonov A, Piano A, Svistkova V, Titorenko VI. Lithocholic bile acid accumulated in yeast mitochondria orchestrates a development of an anti-aging cellular pattern by causing age-related changes in cellular proteome. Cell Cycle. 2015; 14:1643-1656.

Cabib E, Arroyo J. How carbohydrates sculpt cells: chemical control of morphogenesis in the yeast cell wall. Nat Rev Microbiol. 2013; 11:648-655.

Conrad M, Schothorst J, Kankipati HN, Van Zeebroeck G, Rubio-Texeira M, Thevelein JM. Nutrient sensing and signaling in the yeast Saccharomyces cerevisiae. FEMS Microbiol Rev. 2014; 38:254-99.

Davidson GS, Joe RM, Roy S, Meirelles O, Allen CP, Wilson MR, Tapia PH, Manzanilla EE, Dodson AE, Chakraborty S, Carter M, Young S, Edwards B, Sklar L, Werner-Washburne M. The proteomics of quiescent and non-quiescent cell differentiation in yeast stationary-phase cultures. Mol Biol Cell. 2011; 22:988-998.

Deprez MA, Eskes E, Winderickx J, Wilms T. The TORC1-Sch9 pathway as a crucial mediator of chronological lifespan in the yeast Saccharomyces cerevisiae. FEMS Yeast Res. 2018; 18: foy048.

De Virgilio C. The essence of yeast quiescence. FEMS Microbiol Rev. 2012; 36:306-339.

Fraenkel DG. Yeast intermediary metabolism; Cold Spring Harbor Laboratory Press: Cold Spring Harbor, NY, USA, 2011; ISBN 978-0-87969-797-6.

François J, Parrou JL. Reserve carbohydrates metabolism in the yeast Saccharomyces cerevisiae. FEMS Microbiol Rev. 2001; 25:125-145.

Goldberg AA, Bourque SD, Kyryakov P, Gregg C, Boukh-Viner T, Beach A, Burstein MT, Machkalyan G, Richard V, Rampersad S, Cyr D, Milijevic S, Titorenko VI. Effect of calorie restriction on the metabolic history of chronologically aging yeast. Exp Gerontol. 2009; 44:555-571.

Goldberg AA, Richard VR, Kyryakov P, Bourque SD, Beach A, Burstein MT, Glebov A, Koupaki O, Boukh-Viner T, Gregg C, Juneau M, English AM, Thomas DY, Titorenko VI. Chemical genetic screen identifies lithocholic acid as an anti-aging compound that extends yeast chronological life span in a TOR-independent manner, by modulating housekeeping longevity assurance processes. Aging (Albany NY). 2010; 2:393-414.

Gladyshev VN. The origin of aging: imperfectness-driven non-random damage defines the aging process and control of lifespan. Trends Genet. 2013; 29:506-512.

Giorgio M, Trinei M, Migliaccio E, Pelicci PG. Hydrogen peroxide: a metabolic by-product or a common mediator of ageing signals? Nat Rev Mol Cell Biol. 2007; 8:722-728.

Gulli J, Cook E, Kroll E, Rosebrock A, Caudy A, Rosenzweig F. Diverse conditions support near-zero growth in yeast: Implications for the study of cell lifespan. Microb Cell. 2019; 6:397-413.

He K, Gkioxari G, Dollar P, Girshes R. Mask R-CNN. IEEE Trans Pattern Anal Mach Intell. 2020; 42:386-397.

Herker E, Jungwirth H, Lehmann KA, Maldener C, Fröhlich KU, Wissing S, Büttner S, Fehr M, Sigrist S, Madeo F. Chronological aging leads to apoptosis in yeast. J Cell Biol. 2004; 164:501-507.

Kaeberlein M, Burtner CR, Kennedy BK. Recent developments in yeast aging. PLoS Genet. 2007; 3: e84.

Kyryakov P, Beach A, Richard VR, Burstein MT, Leonov A, Levy S, Titorenko VI. Caloric restriction extends yeast chronological lifespan by altering a pattern of age-related changes in trehalose concentration. Front Physiol. 2012; 3: 256.

Leonov A, Feldman R, Piano A, Arlia-Ciommo A, Lutchman V, Ahmadi M, Elsaser S, Fakim H, Heshmati-Moghaddam M, Hussain A, Orfali S, Rajen H, Roofigari-Esfahani N, Rosanelli L, Titorenko VI. Caloric restriction extends yeast chronological lifespan via a mechanism linking cellular aging to cell cycle regulation, maintenance of a quiescent state, entry into a non-quiescent state and survival in the non-quiescent state. Oncotarget. 2017; 8:69328-69350.

Leonov A, Titorenko VI. A network of interorganellar communications underlies cellular aging. IUBMB Life. 2013; 65:665-674.

Longo VD. Mutations in signal transduction proteins increase stress resistance and longevity in yeast, nematodes, fruit flies, and mammalian neuronal cells. Neurobiol Aging. 1999; 20: 479-486.

Longo VD, Shadel GS, Kaeberlein M, Kennedy B. Replicative and chronological aging in Saccharomyces cerevisiae. Cell Metab. 2012; 16:18-31.

Madeo F, Carmona-Gutierrez D, Hofer SJ, Kroemer G. Caloric Restriction Mimetics against Age-Associated Disease: Targets, Mechanisms, and Therapeutic Potential. Cell Metab. 2019; 29:592-610.

Lu AX, Zarin T, Hsu IS, Moses AM. YeastSpotter: accurate and parameter-free web segmentation for microscopy images of yeast cells. Bioinformatics. 2019; 35:4525-4527.

Miles S, Li L, Davison J, Breeden LL. Xbp1 directs global repression of budding yeast transcription during the transition to quiescence and is important for the longevity and reversibility of the quiescent state. PLoS Genet. 2013; 9: e1003854.

Miles S, Li LH, Melville Z, Breeden LL. Ssd1 and the cell wall integrity pathway promote entry, maintenance, and recovery from quiescence in budding yeast. Mol Biol Cell. 2019; 30:2205-2217.

Mitrofanova D, Dakik P, McAuley M, Medkour Y, Mohammad K, Titorenko VI. Lipid metabolism and transport define longevity of the yeast Saccharomyces cerevisiae. Front Biosci (Landmark Ed). 2018; 23:1166-1194.

Ogrodnik M, Salmonowicz H, Gladyshev VN. Integrating cellular senescence with the concept of damage accumulation in aging: Relevance for clearance of senescent cells. Aging Cell. 2019; 18: e12841.

Palková Z, Wilkinson D, Váchová L. Aging and differentiation in yeast populations: elders with different properties and functions. FEMS Yeast Res. 2014; 14:96-108.

Powers RW 3rd, Kaeberlein M, Caldwell SD, Kennedy BK, and Fields S. Extension of chronological life span in yeast by decreased TOR pathway signaling. Genes Dev. 2006; 20: 174-184.

Richard VR, Beach A, Piano A, Leonov A, Feldman R, Burstein MT, Kyryakov P, Gomez-Perez A, Arlia-Ciommo A, Baptista S, Campbell C, Goncharov D, Pannu S, Patrinos D, Sadri B, Svistkova V, Victor A, Titorenko VI. Mechanism of liponecrosis, a distinct mode of programmed cell death. Cell Cycle. 2014; 13):3707-3726.

Sagot I, Laporte D. The cell biology of quiescent yeast - a diversity of individual scenarios. J Cell Sci. 2019; 132: jcs213025.

Shashkova S, Welkenhuysen N, Hohmann S. Molecular communication: crosstalk between the Snf1 and other signaling pathways. FEMS Yeast Res. 2015; 15: fov026.

Sheibani S, Richard VR, Beach A, Leonov A, Feldman R, Mattie S, Khelghatybana L, Piano A, Greenwood M, Vali H, Titorenko VI. Macromitophagy, neutral lipids synthesis, and peroxisomal fatty acid oxidation protect yeast from “liponecrosis”, a previously unknown form of programmed cell death. Cell Cycle. 2014; 13:138-147.

Sinclair DA. Toward a unified theory of caloric restriction and longevity regulation. Mech Ageing Dev. 2005; 126:987-1002.

Smets B, Ghillebert R, De Snijder P, Binda M, Swinnen E, De Virgilio C, Winderickx J. Life in the midst of scarcity: adaptations to nutrient availability in Saccharomyces cerevisiae. Curr Genet. 2010; 56:1-32.

Swinnen E, Ghillebert R, Wilms T, Winderickx J. Molecular mechanisms linking the evolutionary conserved TORC1-Sch9 nutrient signalling branch to lifespan regulation in Saccharomyces cerevisiae. FEMS Yeast Res. 2014; 14:17-32.

Werner-Washburne M, Roy S, Davidson GS. Aging and the survival of quiescent and non-quiescent cells in yeast stationary-phase cultures. Subcell Biochem. 2012; 57:123-143.

Zhang L, Winkler S, Schlottmann FP, Kohlbacher O, Elias JE, Skotheim JM, Ewald JC. Multiple Layers of Phospho-Regulation Coordinate Metabolism and the Cell Cycle in Budding Yeast. Front Cell Dev Biol. 2019;7: 338.

Chapter 6: Supplemental Material

6.1 DIC micrographs of the Q^{HD} and Q^{LD} cell populations purified by centrifugation in Percoll density and recovered from different phases of culturing

(A) Day 1 (L)

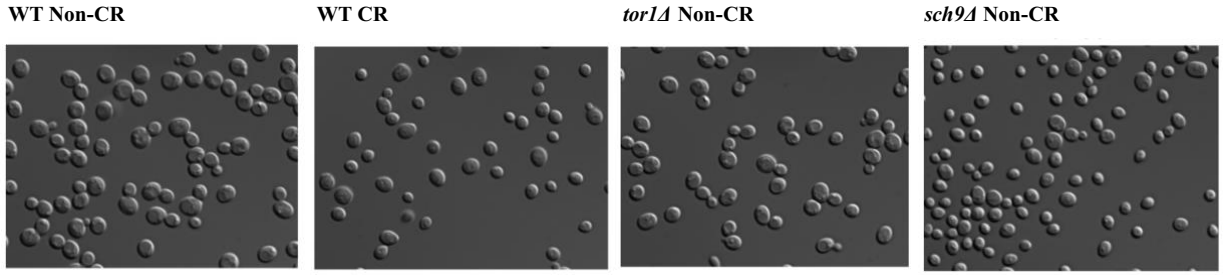

(B) Day 2 (D)

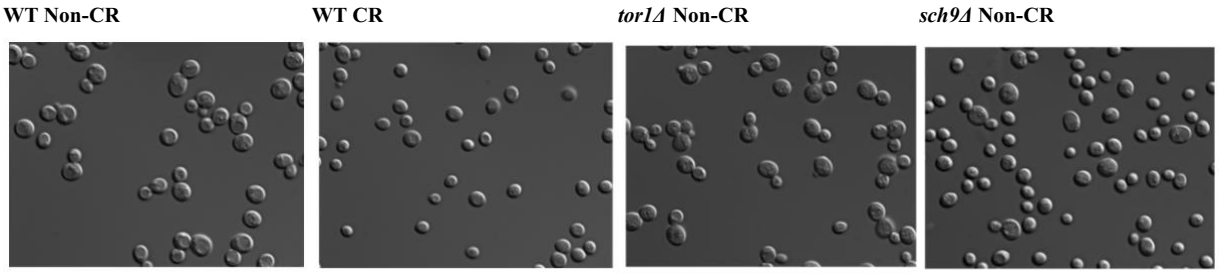

(C) Day 3 (D)

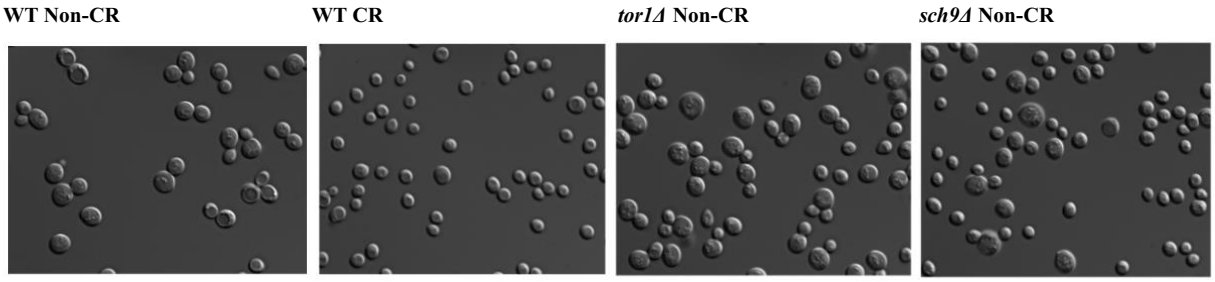

(D) Day 5 (PD)

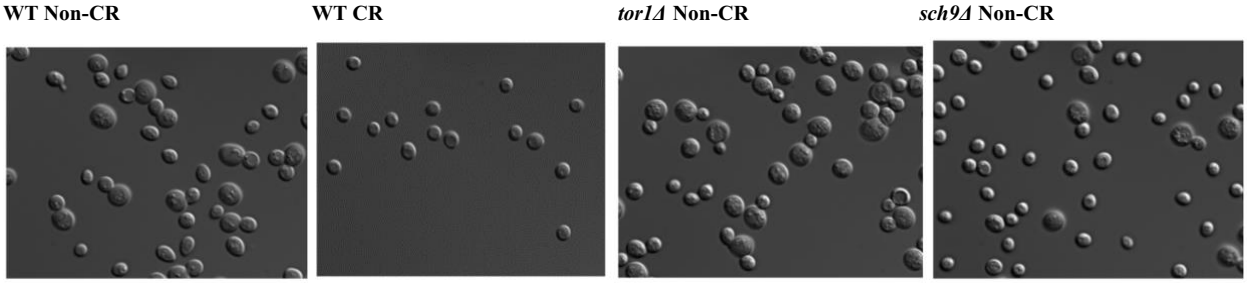

(E) Day 7 (ST)

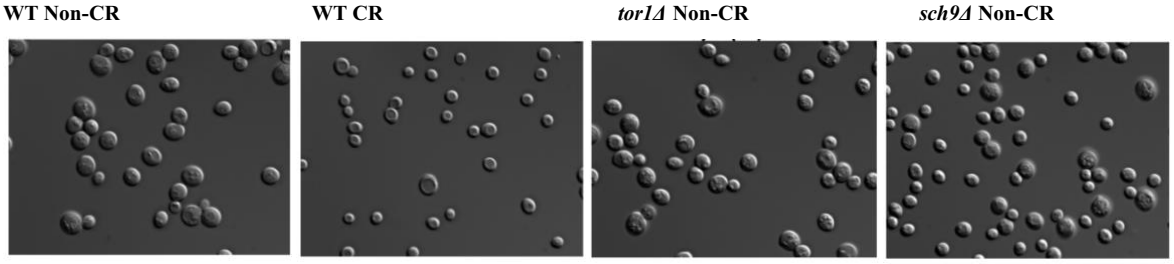

(F) Day 10 (ST)

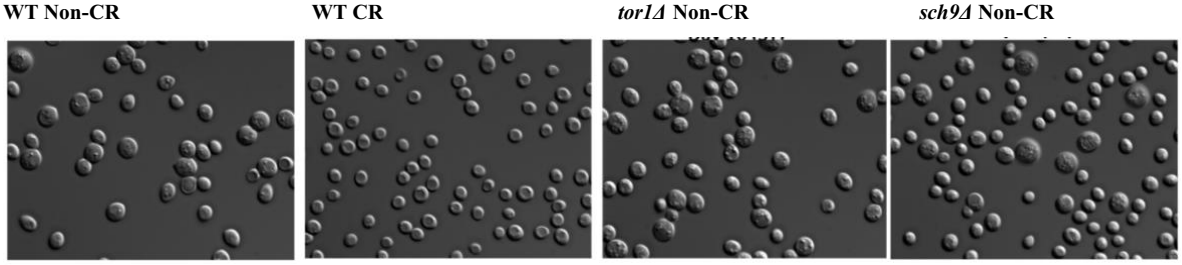

(G) Day 14 (ST)

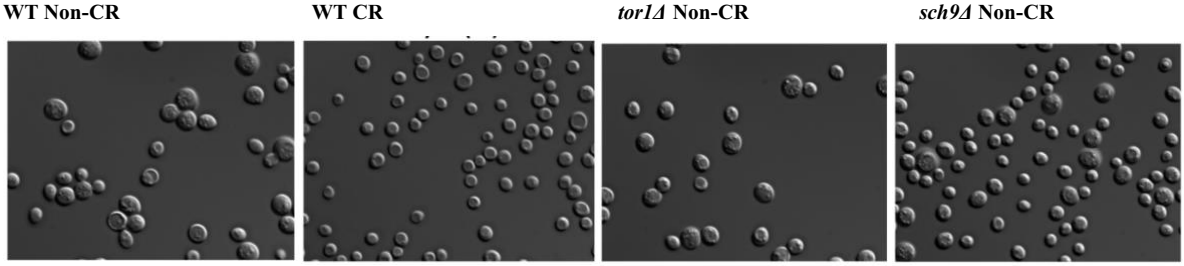

(H) Day 17 (ST)

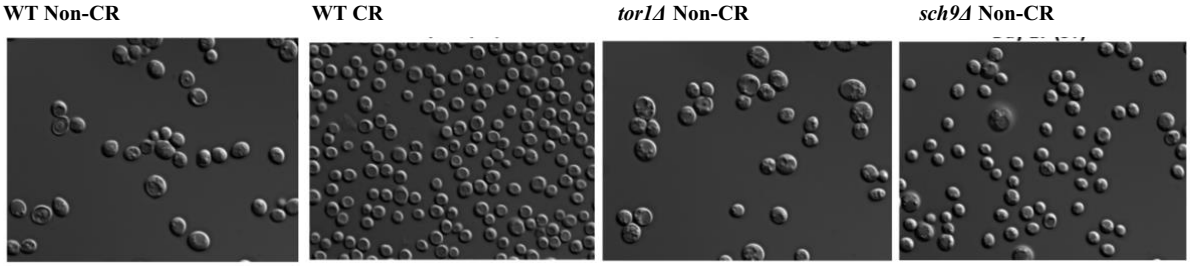

(I) Day 21 (ST)

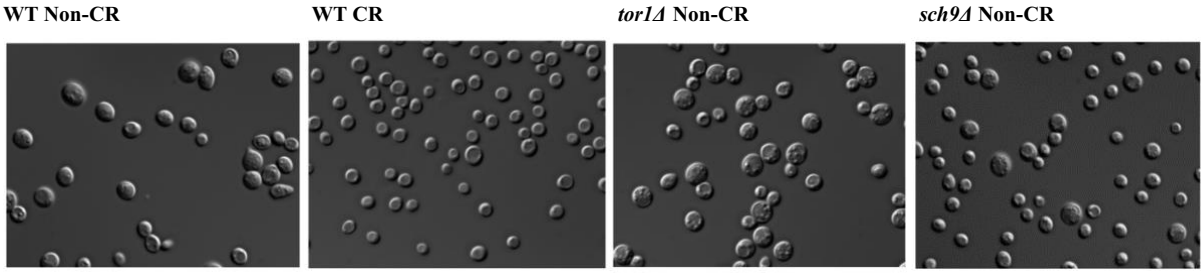

Figure 6.1: DIC micrographs of the Q^{HD} cell populations purified by centrifugation in Percoll density gradient from WT non-CR, WT CR, *tor1Δ*, and *sch9Δ* non-CR cells recovered from different phases of culturing. Samples of WT yeast cultured in the nutrient-rich YP medium initially containing 2% glucose (non-CR) were retrieved from logarithmic (L), diauxic (D), post-diauxic (PD) or stationary (ST) phase of culturing. These samples were then subjected to centrifugation in Percoll density gradient. The Q^{HD} cell populations were recovered and subjected to the DIC. Other abbreviations: DIC, differential interference contrast; HD, high-density cells; Q, quiescent cells.

(A) Day 1 (L)

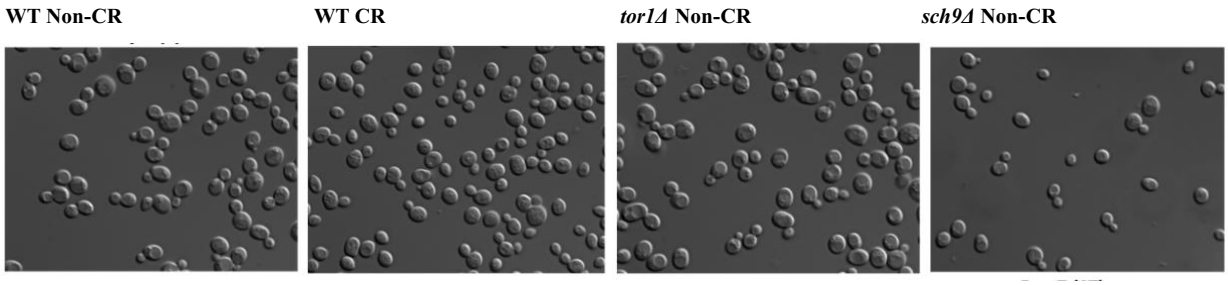

(B) Day 2 (D)

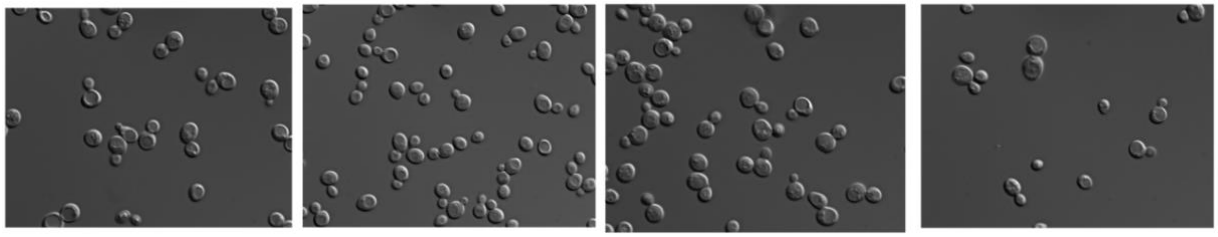

(C) Day 3 (D)

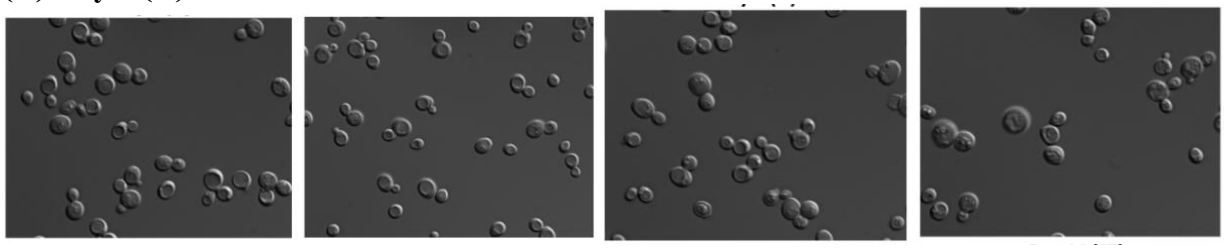

(D) Day 5 (PD)

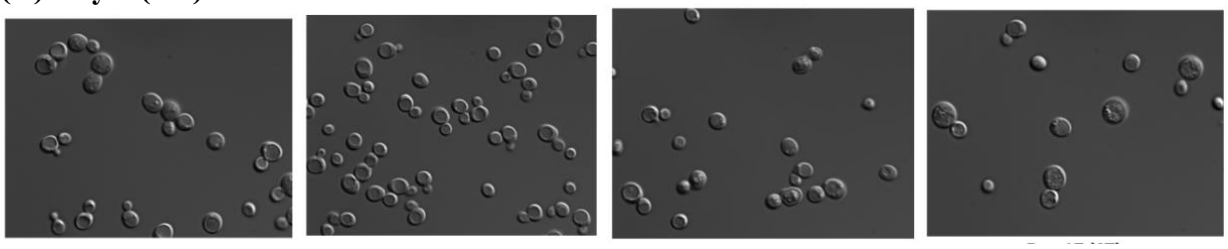

(E) Day 7 (ST)

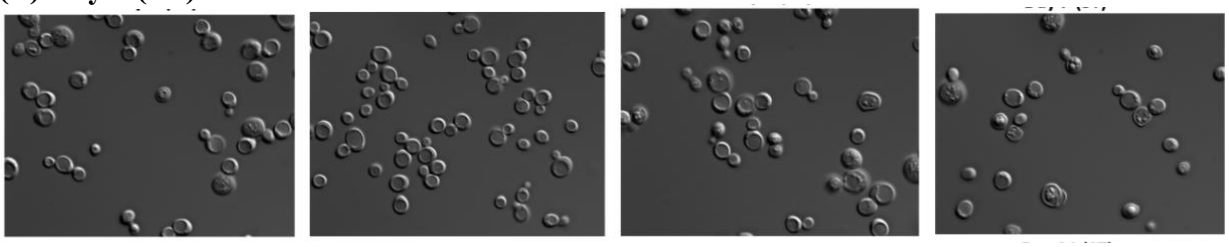

(F) Day 10 (ST)

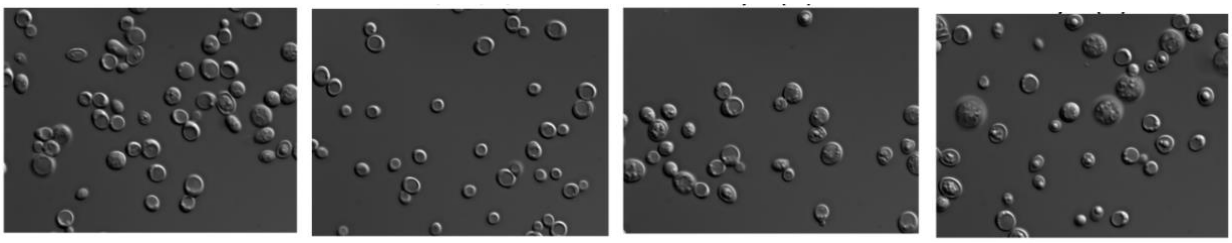

(G) Day 14 (ST)

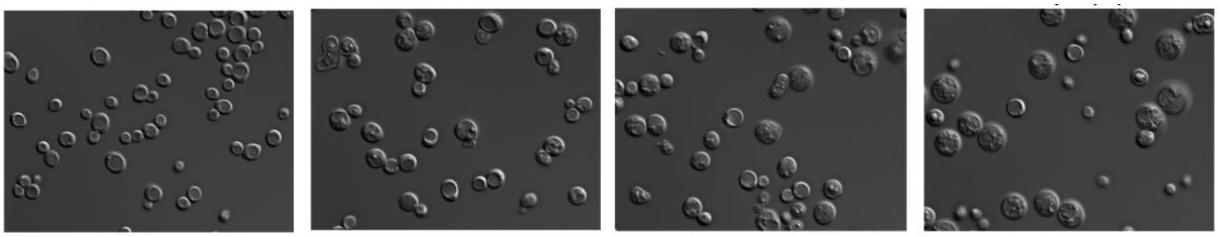

(H) Day 17 (ST)

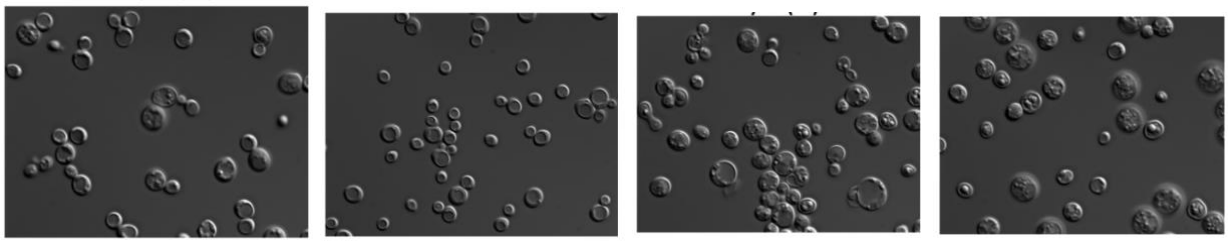

(I) Day 21 (ST)

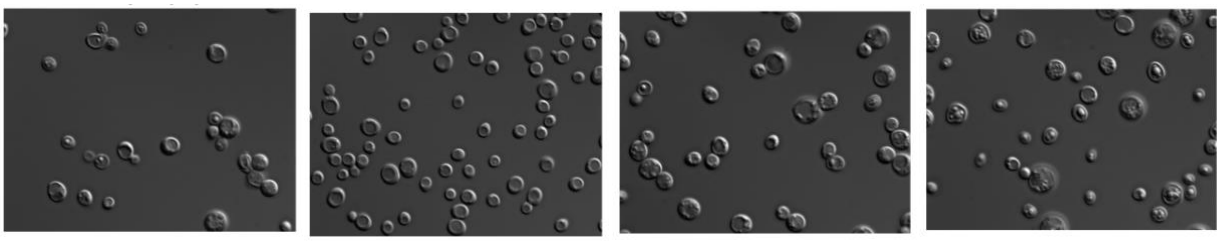

Figure 6.2: DIC micrographs of the Q^{LD} cell populations purified by centrifugation in Percoll density gradient from WT non-CR, WT CR, *tor1Δ*, and *sch9Δ* non-CR cells recovered from different phases of culturing. Samples of WT yeast cultured in the nutrient-rich YP medium initially containing 0.2% glucose (CR) were retrieved from logarithmic (L), diauxic (D), post-diauxic (PD) or stationary (ST) phase of culturing. These samples were then subjected to centrifugation in Percoll density gradient. The Q^{LD} cell populations were recovered and subjected to the DIC. Abbreviation: Other abbreviation: DIC, differential interference contrast; LD, low-density cells; Q, quiescent cells.

6.2 Average cell diameters of group 1 and group 2, HD and LD, *sch9Δ* cells under non-CR

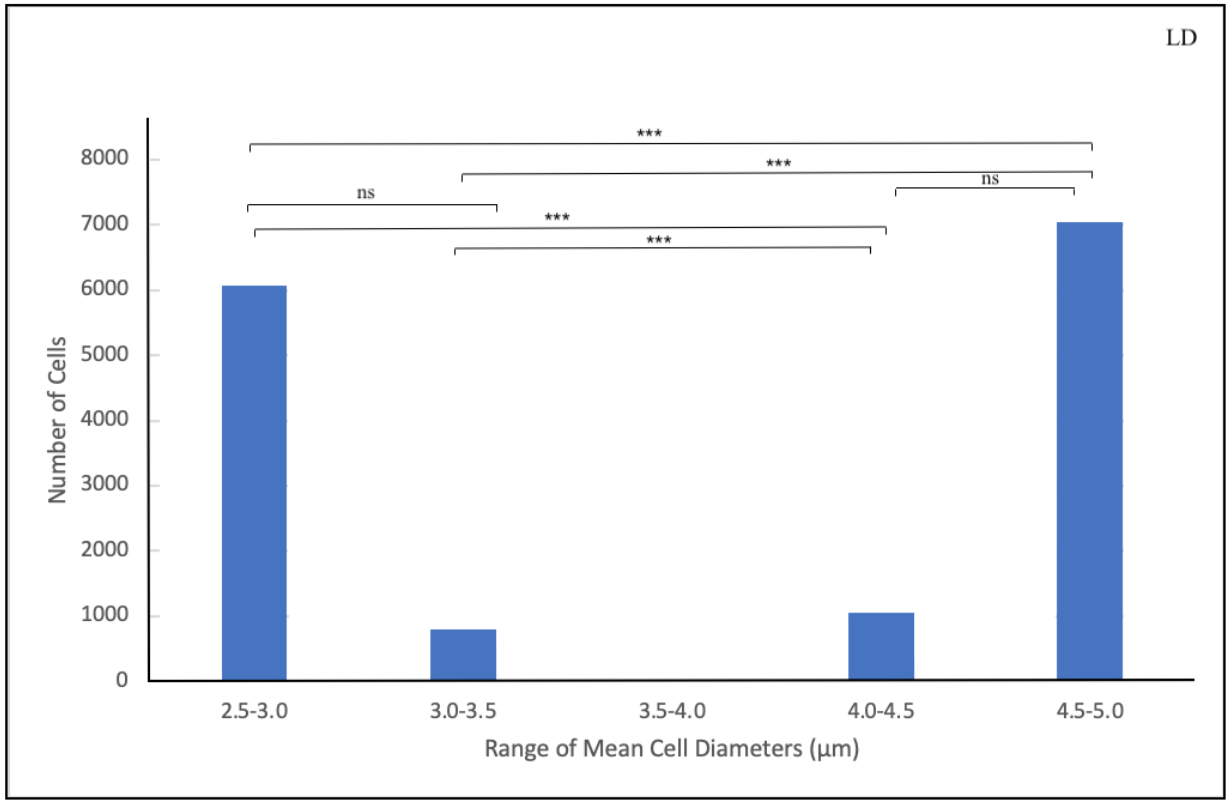

Figure 6.3: Number of LD *sch9Δ* cell population and sizes (mean diameters) under non-CR, recovered from different phases of culturing, subjected to DIC and comparative morphometric analysis. Yeast *sch9Δ* cultured in the nutrient-rich YP medium initially containing 2% glucose (non-CR). Cell aliquots were recovered on different days of culturing. These aliquots were then subjected to centrifugation in a Percoll density gradient. The purified LD cell fraction was subjected to DIC imaging to assess their cell diameters. Average cell diameter range of 2.5-3.5 µm was named as group 1 and average cell diameter range of 4.0-5.0 µm was named group 2. ($n = 3$; *$p < 0.05$; **$p < 0.01$; ***p < 0.001). Abbreviations: LD, low-density cells.

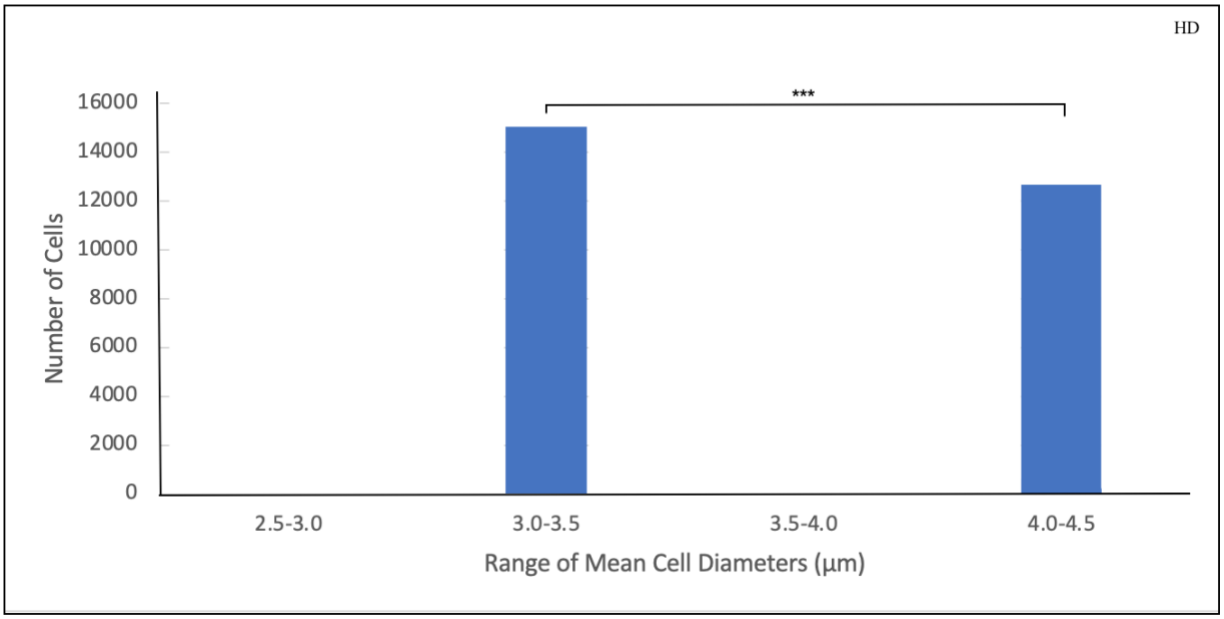

Figure 6.4: Number of HD *sch9Δ* cell populations and sizes (mean diameters) under non-CR, recovered from different phases of culturing, subjected to DIC and comparative morphometric analysis. Yeast *sch9Δ* cultured in the nutrient-rich YP medium initially containing 2% glucose (non-CR). Cell aliquots were recovered on different days of culturing. These aliquots were then subjected to centrifugation in a Percoll density gradient. The purified HD cell fraction was subjected to DIC imaging to assess their cell diameters. Average cell diameter range of 3.0-3.5 µm was named as group 1 and average cell diameter range of 4.0-4.5 µm was named group 2. ($n = 3$; *$p < 0.05$; **$p < 0.01$; ***$p < 0.001$). Abbreviations: HD, high-density cells.